

FINAL TECHNICAL REPORT
Award Number: G13AP00030

Title: “Developing Empirical GMPEs for Eastern North America based on the NGA East Ground Motion Database and Additional M6-7 Ground Motion Estimates from Historical Earthquake Intensities”

Chris H. Cramer, Md. Nayeem Al Noman, and Luke Philip Ogwen

Center for Earthquake Research and Information

University of Memphis

3890 Central Ave

Memphis, TN 38152-3050

901-678-4992

FAX: 901-678-4734

cramer@ceri.memphis.edu

June 1, 2013 – May 31, 2014

Submitted: August 31, 2014

“Research supported by the U.S. Geological Survey (USGS), Department of Interior, under USGS award number G13AP00030. The views and conclusions contained in this document are those of the authors and should not be interpreted as necessarily representing the official policies, either expressed or implied, of the U.S. Government.”

Abstract

The Next Generation Attenuation (NGA) East database of ground motions for eastern North America (ENA) contains over 10,000 records (horizontal and/or vertical) from 85 earthquakes in the magnitude range $M_{2.2-7.6}$. Distance coverage is good to less than 10 km for $M < 6.0$, but empirical observations are still poor for $M \geq 6.0$. Nonetheless, the empirical dataset provided by the NGA East ground motion database is much improved over that of a decade ago and similar to that in California a couple of decades ago. An initial regression has been performed using both one- and two-stage approaches and comparisons made with current ENA GMPEs (Al Noman, 2013). Below M_6 the comparisons with current ENA GMPEs suggests that the NGA East ground motion database predicts ground motion levels similar to current GMPEs at short periods and lower than current GMPEs at long periods. We have improved the Al Noman (2013) empirical ENA GMPEs adding ground motion estimates from intensity observations to better constrain the GMPEs for $M > 6$. Dangkua and Cramer (2011) provide estimates of median ground motion with uncertainty for a given level of Modified Mercalli Intensity (MMI) in ENA. For a given historical earthquake, median distance and its uncertainty for a given level of MMI can be associated with the Dangkua and Cramer (2011) median ground motion level for that MMI. For the 1988 $M_{5.9}$ Saguenay and 2011 $M_{5.7}$ Mineral, Virginia earthquakes, ground motion levels estimated in this manner from intensities compare very well with actual ground motion observations, even at close in distances (< 100 km), suggesting that this is a viable and valuable approach to add additional empirical constrains at large magnitudes. To increase the number of available intensity observations at close-in distances, MMI observations are converted to median ground motion estimates. The Dangkua and Cramer (2011) relations have been updated with additional ground motion vs. intensity information and by applying a correction of more recent Community Internet Intensity (CII) observations to MMI. Additionally, uncertainty in magnitude estimates for some large historical earthquakes are still large, but Cramer and Boyd (2014) provide a means of better constraining these magnitude estimates by comparing mean MMI estimates at large distances with similar estimates for earthquakes with known magnitudes. Also a V_{s30} site term has been added to the GMPE regression and V_{s30} soil classifications estimated using ground motion and intensity site locations. Developing empirical GMPEs for ENA that include historical intensity observations better constrains the empirical GMPE above $M 6.0$, improves our empirical understanding of ENA magnitude and V_{s30} scaling, and suggests the inappropriateness of including the 2011 $M_{7.6}$ Bhuj, India long-period ground motion observations in the empirical GMPE inversion.

Introduction

Earthquake ground motion prediction equations (GMPEs) are an important component of earthquake hazard analyses. Over the years many eastern North America (ENA) GMPEs have been developed and refined. Currently, the U. S. Nuclear Regulatory Commission (NRC), the U.S. Department of Energy (DOE), the Electric Power Research Institute (EPRI), and the U.S. Geological Survey (USGS) are funding and supporting the Next Generation Attenuation (NGA) East project by the Pacific Earthquake Engineering Research (PEER) Center to develop new ENA GMPEs. As a part of the NGA East project, NRC at first and then PEER has funded the development of a NGA East ground motion database (Cramer et al., 2009, 2010, 2011) that contains over 10,000 records (horizontal and/or vertical component) from 85 earthquake and covering the magnitude range of $M_{2.2} - 7.6$. Figure 1 shows the magnitude versus distance distribution of the NGA East ground motion database. Distance coverage is good to less than 10 km for $M < 6.0$, but observations are still sparse above $M_{6.0}$.

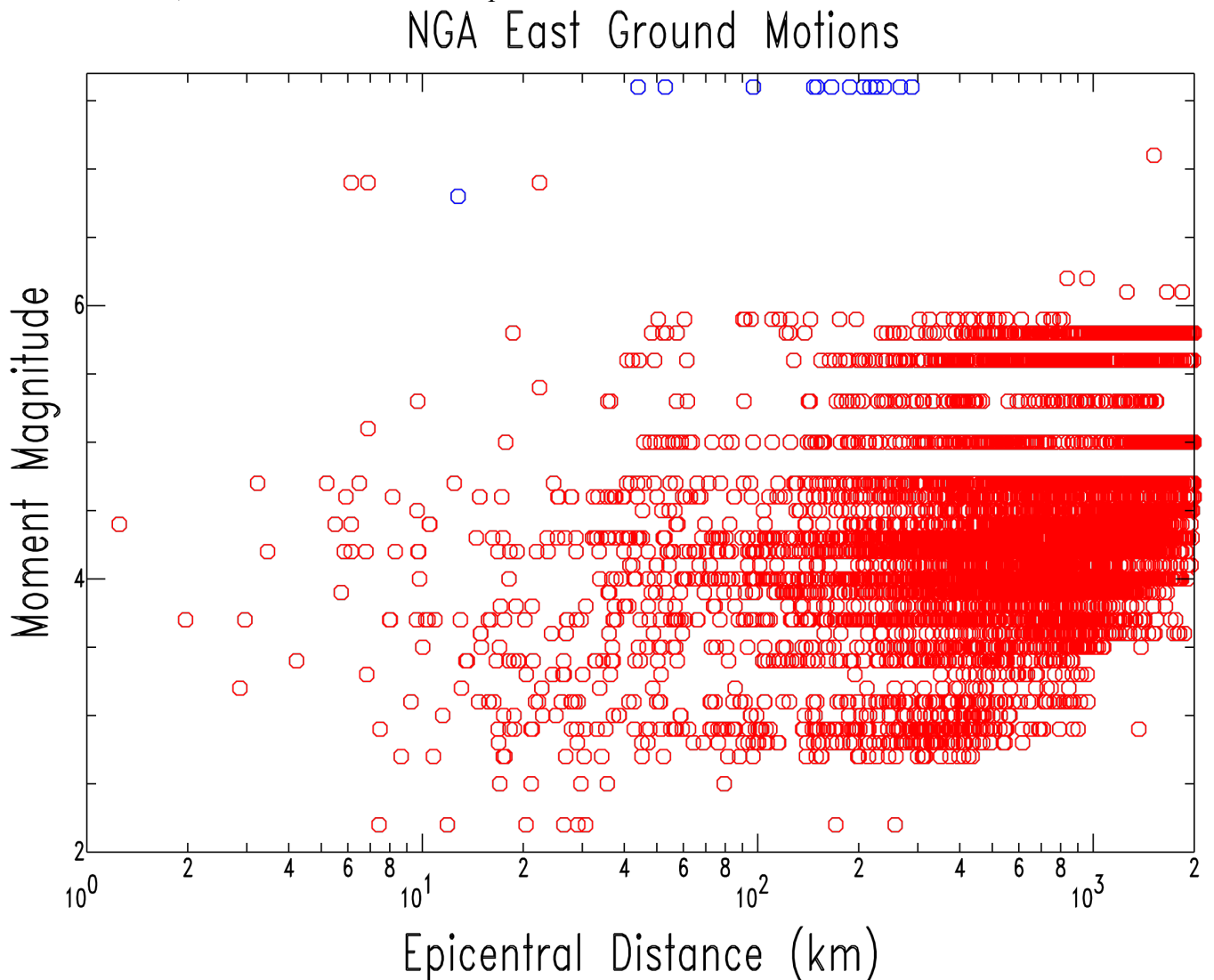


Figure 1: NGA East distance vs. magnitude plot for all observations. Red circles are for ENA observations and blue circles are for Bhuj, India and Gazli, USSR observations.

The NGA East ground motion database is a great improvement from similar databases from a decade ago and resembles California databases from a couple of decades ago. Some M7 data from two stable continental region (SCR) earthquakes (the 2001 M7.7 Bhuj, India and 1976 M6.8 Gazli, USSR earthquakes) plus the close-in observations from the 1985 M6.9 Nahanni, Canada earthquake are included in the NGA East database to help constrain ground motion observations at large magnitudes. However additional empirical constraints at large magnitudes would be helpful.

Developing empirical GMPEs for ENA can also be used to explore and define the trends and limitations of the NGA East ground motion database, beyond the obvious limitation of a lack of observations above M6.0. An initial empirical GMPE by Al Noman (2013) as well as comparisons for individual M5-6 events to currently available GMPEs (Cramer et al., 2009, 2010, 2011) have shown that current GMPEs as a group generally predict observed ground motions at short periods (PGA and 0.2s Sa) but over predict observations at long periods (1.0s Sa) – Figures 2 and 3. Other issues that can be explored are the limits of site condition coverage (including Vs30), the effect of earthquake source parameters (focal mechanism and stress drop), and inconsistency among recordings at each station.

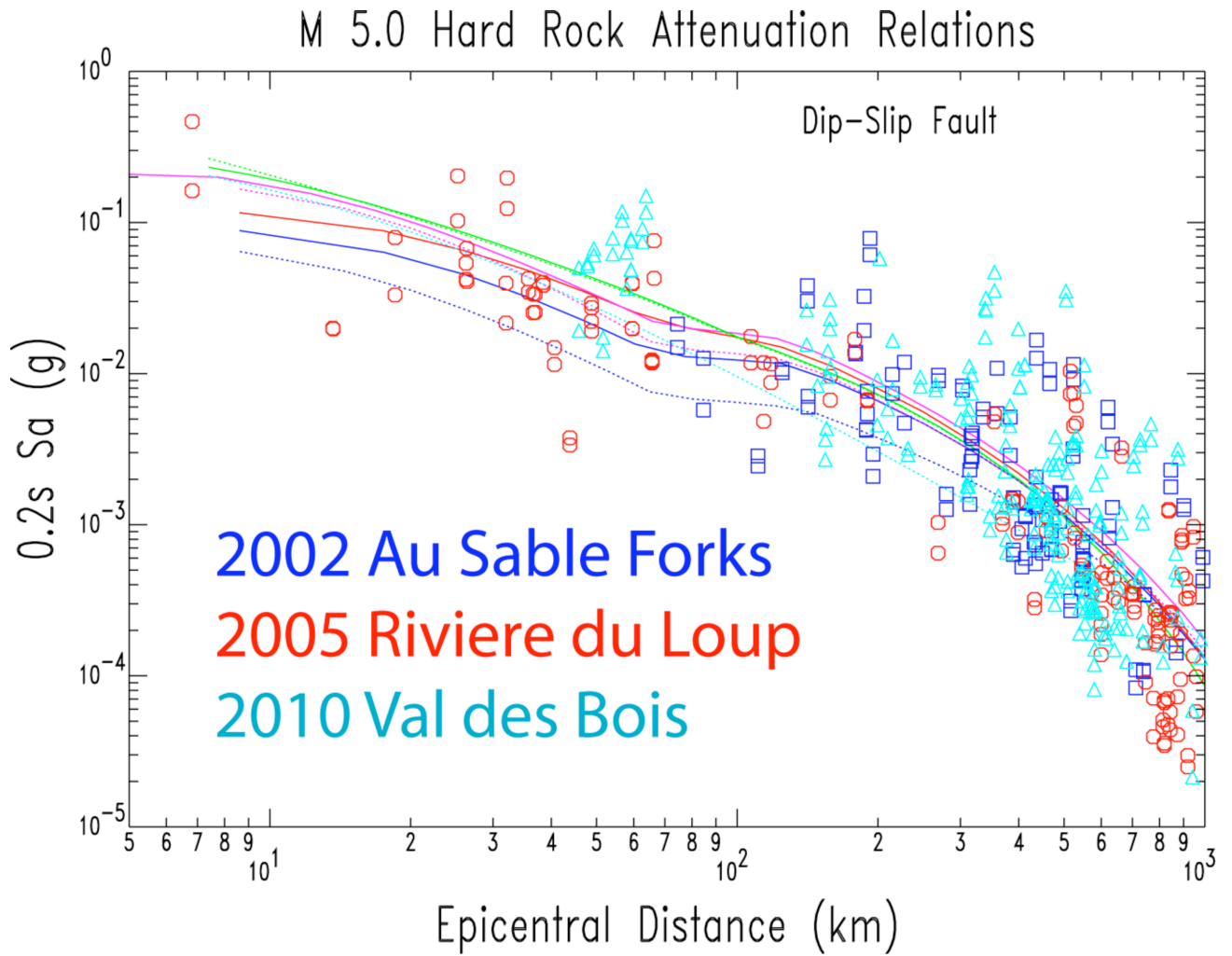


Figure 2: Comparison at 0.2 s spectral acceleration of M5 observations from the NGA East database with current ENA GMPEs for M5.0 showing similar levels of ground motion. Data from some soil sites are included, which show larger than expected ground motions.

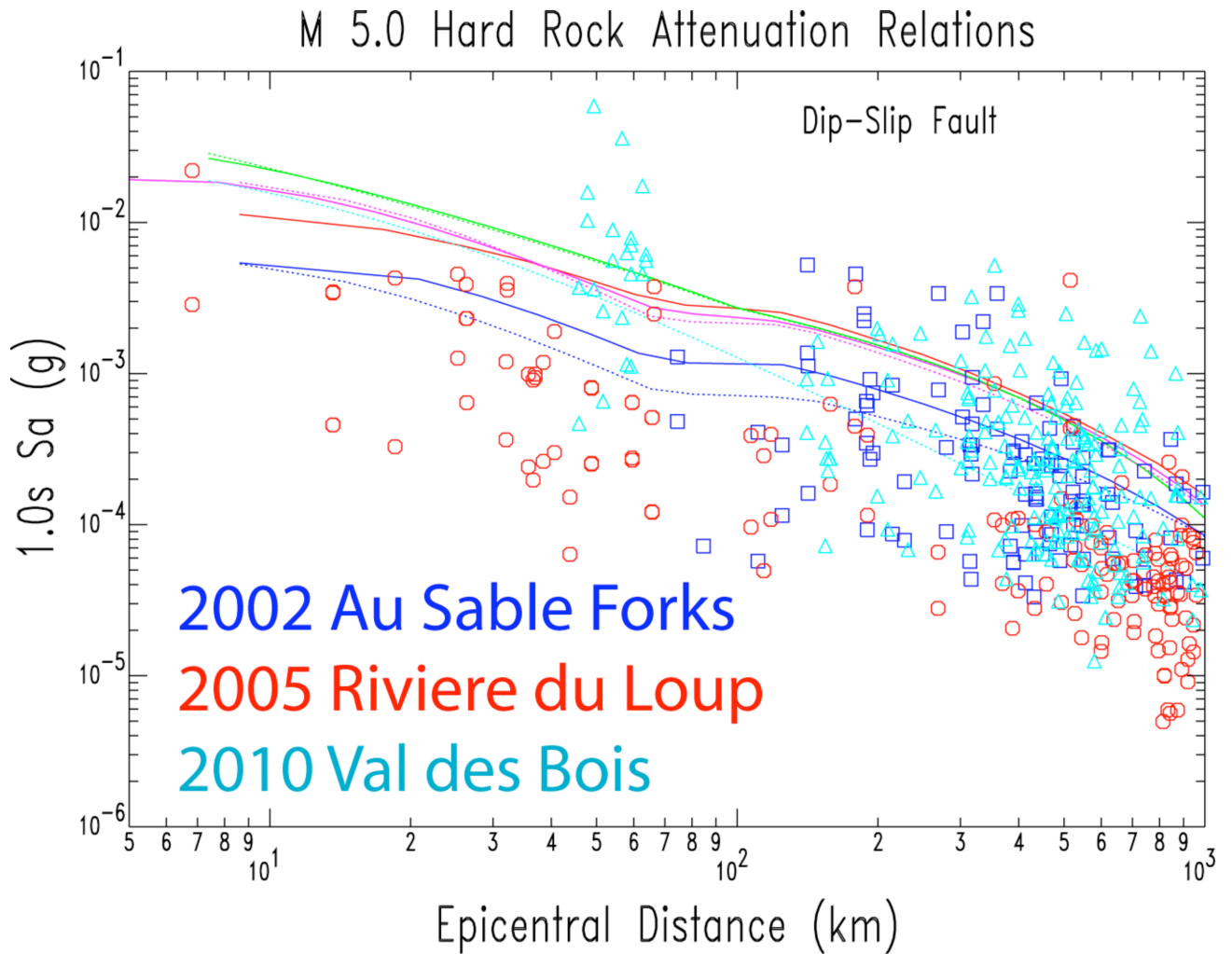


Figure 3: Comparison at 1.0 s spectral acceleration of M5 observations from the NGA East database with current ENA GMPEs for M5.0 showing over prediction of levels of ground motion by current GMPEs. Data from some soil sites are included, which show larger than expected ground motions.

Methodologies

Regression: In an initial analysis, Al Noman (2013) started with a simple functional form consisting of magnitude and distance dependent terms for the observed ground motion. They used a quadratic magnitude dependent polynomial, adding style of faulting terms as a dummy variables (UU,RR,SS), a magnitude (M) dependent geometrical spreading, and anelastic attenuation terms for the distance (R) dependence. The initial prediction equation is

$$\log Y = b_1*UU + b_2*RR + b_3*SS + b_4*M + b_5*M^2 + (c_1 + c_2*M)*\log(\sqrt{R^2 + h^2}) + c_3*\sqrt{R^2 + h^2}, \quad (1)$$

where Y is the observed ground motion in g ; and b_1 through b_5 , c_1 through c_3 , and h are regression coefficients; and UU , RR , SS are dummy variables for Unspecified, Reverse, and Strike slip mechanisms respectively that take a value of 1 for their own mechanism and 0 otherwise. An additional $Vs30$ term has been added to equation 1 in this study in place of the original three site condition alternatives of Al Noman (2013): $+ d_1 * \log(Vs30/760)$.

The regression equation (1) can be represented by a linear system

$$A = XB + \sigma, \quad (2)$$

where A represents the matrix of $\ln Y$, B is the matrix of regression coefficients for equation (1), and σ is the standard error of the $\ln Y$ estimate [composed of within-event aleatory uncertainty, ϕ , and between-event aleatory uncertainty, τ , and is defined as $\sigma = \sqrt{\phi^2 + \tau^2}$]. Al Noman (2013) used both a one-stage maximum likelihood method and a two-stage method (Joyner and Boore, 1993, 1994) to find the regression coefficient matrix B of this linear system.

In the one-stage method, the parameters are all determined simultaneously by maximizing the likelihood of the set of observations, i.e. $\ln Y$. The components of σ are assumed to be normally distributed with zero mean and variance-covariance matrix V of the system. According to the maximum likelihood method, the likelihood of the sample of observation is

$$L = (2\pi)^{-N/2} |V|^{-1/2} \exp[-0.5*(A - XB)^T V^{-1} (A - XB)], \quad (3)$$

where N is the total number of records. Maximizing L with respect to B , the solution becomes

$$B = (X^T V^{-1} X)^{-1} X^T V^{-1} A. \quad (4)$$

As the records from the same earthquake are taken consecutively, the variance-covariance matrix V becomes a block diagonal matrix with each block corresponding to an earthquake. Again, as V depends on σ , we iterated the value of σ , weighting each earthquake component in the matrix V to maximize L and find the corresponding regression coefficient B for the system.

Using this method we can only solve for the value of total σ , but cannot separate out the within-event aleatory uncertainty, ϕ , from the between-event aleatory uncertainty, τ . However, the two-stage method described below allows us to estimate both uncertainties and is the method used in this study.

In the two-stage method, the magnitude and distance dependencies are analyzed separately to get the within-event aleatory uncertainty, ϕ , and the between-event aleatory uncertainty, τ . In the first stage, the parameter controlling distance dependence and a set of event terms, one for each earthquake, are determined by maximizing the likelihood of the set of observations ($\ln Y$) in equation (1). The parameters controlling magnitude dependence are then computed in the second stage by maximizing the likelihood of the set of event terms found in the first stage.

In the first stage the observational data are regressed against distance considering the added event term $b_0(\text{event})$ for each earthquake using equation (5):

$$\ln Y = b_0(\text{event}) + (c_1 + c_2 * M) * \ln(\sqrt{R^2 + h^2}) + c_3 * \sqrt{R^2 + h^2}. \quad (5)$$

In this equation $b_0(\text{event})$ is shorthand for the sum: $(b_0)_1\delta_1 + (b_0)_2\delta_2 + \dots + (b_0)_{NE}\delta_{NE}$, where $(b_0)_j\delta_j$ is the event term for event j , δ_j equals 1 for event j and zero otherwise, and NE is the number of earthquakes.

The regression coefficients $b_0(\text{event})$, c_1 , c_2 , and c_3 are found by ordinary least squares regression. This stage gives the corresponding within-event aleatory uncertainty, ϕ , following the regression.

The event terms found in the first stage are used in the weighted second stage regression to determine the magnitude scaling of the response variables. The regression equation for this stage becomes

$$B_0(\text{event}) = b_1 * UU + b_2 * RR + b_3 * SS + b_4 * M + b_5 * M^2. \quad (6)$$

The component of the weighting matrix used in this stage for each earthquake is considered to have a weight of w_i given by

$$w_i = (\phi^2 / R_i + \tau^2)^{-1}, \quad (7)$$

where R_j is the number of recordings for earthquake j and τ is the between-event aleatory uncertainty associated with this regression equation (6). Magnitude scaling coefficients and τ are determined iteratively to maximize the likelihood of the set of event terms.

Because the available observations less than 40 km are still very few and do not allow us to invert for a different close-in geometrical spreading, we have used a unilinear geometrical spreading term as shown in equation 1. Also the pseudo-depth term h is fixed at 10 km as the available data do not allow for the inversion for h at each ground motion period.

Ground motion from intensity: We associated a median ground motion to each Modified Mercalli intensity (MMI) level in ENA and, for each historical earthquake considered, estimated a median distance for a given MMI. The resulting set of ground motion and distance pairs can be considered as observations for that earthquake in an empirical GMPE regression. Dangkua and Cramer (2011) provide estimates of median ground motion with uncertainty for a given level of Modified Mercalli Intensity (MMI) in ENA. For a given historical earthquake, median distance and its uncertainty for a given level of MMI can be associated with the Dangkua and Cramer (2011) median ground motion level for that MMI. Also the median ground motion level from a ground motion vs. MMI relation, such as Dangkua and Cramer (2011), can be associated with each MMI observation from a historical earthquake, which we chose to do in this study as it takes advantage of observations at distances closer than the median distance for a given MMI.

Additionally, we updated the Dangkua and Cramer (2011) database of ground motion vs. intensity and regressed the ground motion vs. intensity data at additional periods than those used in Dangkua and Cramer (2011). Ground motion vs. intensity observations for the 2011 M5.7

Mineral, VA and the 2011 M5.6 Sparks, OK earthquakes were added to the database. Dangkua and Cramer (2011) only regressed on peak ground acceleration and velocity (PGA and PGV) and at spectral acceleration (Sa) periods of 0.3, 1.0, and 2.0 s. For this study we regressed the Sa data at periods of 0.1, 0.2, 0.3, 0.4, 0.5, 0.6, 0.7, 0.75, 0.8, 0.9, 1.0, 2.0, 3.0, 4.0, 5.0, 6.0, 7.0, 7.5, 8.0, 9.0, and 10.0 s as well as for PGA and PGV. Because NGA East uses the GMrotD50 measure of ground motion, we associated the Dangkua and Cramer (2011) intensity vs. ground motion observations with the recording station for the ground motion observations in order to extract ground motions at additional periods via the NGA East database.

As part of the update of the Dangkua and Cramer (2011) database, we corrected for recently acknowledged differences between CII and MMI (Hough, 2013, 2014). The database contains many CII associations with ground motion for more recent earthquakes as well as MMI associations with ground motion from older earthquakes. We correct (by addition) ENA CII to MMI using the difference between Bakun and Hopper (2004) and Atkinson and Wald (2007) intensity prediction equations (IPEs) for MMI and CII respectively. Similarly for California, we use the difference between Bakun and Wentworth (1997 – equation 6) and Atkinson and Wald (2007) IPEs (MMI and CII respectively). These correction factors were suggested by Sue Hough (Hough, 2014; oral communication, May 3, 2014). Because of the differencing between exponential distributions and Hough’s (2013 – Figure 6) average observed difference of 0.3-0.5 MMI units (depending on data selection) for the 2008 M5.2 Mt. Carmel earthquake, we limited the difference between MMI and CII IPEs to 0.6 MMI units at closer-in distances. Also because MMI should be greater than or equal to CII, we limited negative differences between MMI and CII relations to 0.0 MMI units (at distances beyond 800 km in ENA).

The results of our update of the Dangkua and Cramer (2011) relations for ENA are presented in the Appendix.

Magnitudes of Historical Earthquakes: Uncertainty in magnitude estimates for some large historical earthquakes are still large (range over one unit in magnitude), but Cramer and Boyd (2014) provide a means of better constraining these magnitude estimates by comparing mean MMI estimates at large distances with similar estimates for earthquakes with known magnitudes. We have used the results of Cramer and Boyd (2014) for M7 nineteenth century ENA earthquakes (New Madrid and Charleston, SC) and apply their approach as a check on magnitudes of M6 earthquakes from the nineteenth century.

NGA East Data Selection

In selecting ground motion observations from the NGA East database (Spring 2014 beta version), we avoided known higher attenuating regions in the Gulf Coast and Western US. Thus observations were used from stations and events north of 35°N latitude and east of 100°W longitude. We also included the observations from the 1985 M6.9 Nahanni, NWT Canada earthquake and its large aftershocks, the 1976 M6.8 Gazli, USSR earthquake, and the 2001 M7.6 Bhuj, India earthquake.

Intensity Data Selection

As a check on the MMI to ground motion conversion, we applied the conversion to the 1988 M5.9 Saguenay, Quebec earthquake and the 2011 M5.7 Mineral, Virginia earthquake, which have known ground motions from the NGA East database and a set of intensity measurements from the Geologic Survey of Canada (GSC) (Cajka and Drysdale, 1996) or “Did You Feel It?”. Figure 4 shows the distribution of MMIs with distance and estimates of median distance (mean lognormal distance) and its 95% confidence limits for each MMI level for the Mineral, VA earthquake. The resulting pairs of median distance for each MMI (I – VII) and its associated ENA median peak ground acceleration (PGA) are shown in Figure 5 along with the actual ground motion observations for the Virginia M5.7 earthquake. Figure 6 shows a similar plot for the 1988 M5.9 Saguenay earthquake. The ground motion levels estimated from intensities compare very well with actual ground motion observations, even at close in distances (< 100 km), suggesting that this is a viable and valuable approach to add additional empirical constraints at large magnitudes. At low MMI levels (< III) and large distances (> 500 km), where the observations are sparser and incompletely sampled in both intensity and ground motion with distance, the conversion underestimates the median distance of the median ground motion. However, this is not a big handicap as the estimates from higher MMI levels and closer-in distances are more important for the GMPE regressions.

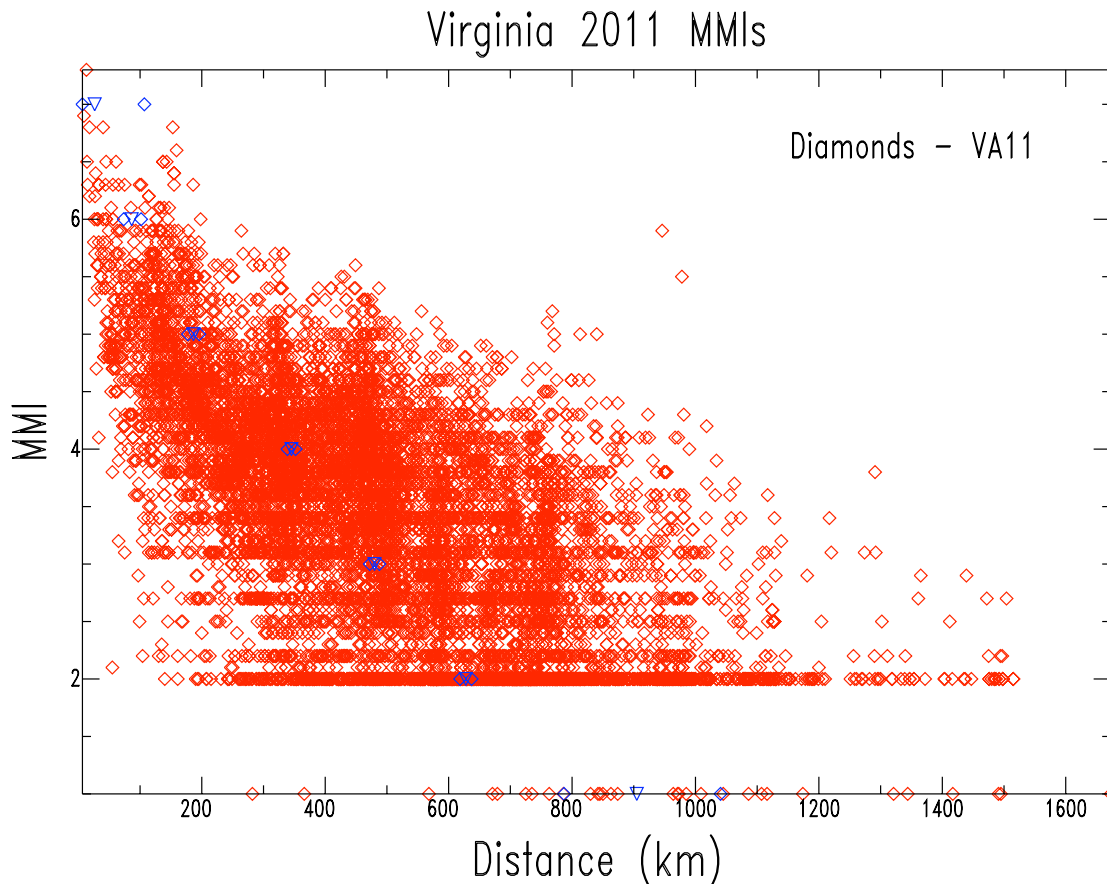


Figure 4: Intensity data (red diamonds) from “Did You Feel It?” for the 2011 M5.7 Mineral, VA earthquake along with estimates of median distance (blue inverted triangle) and their 95% confidence limits (blue diamonds).

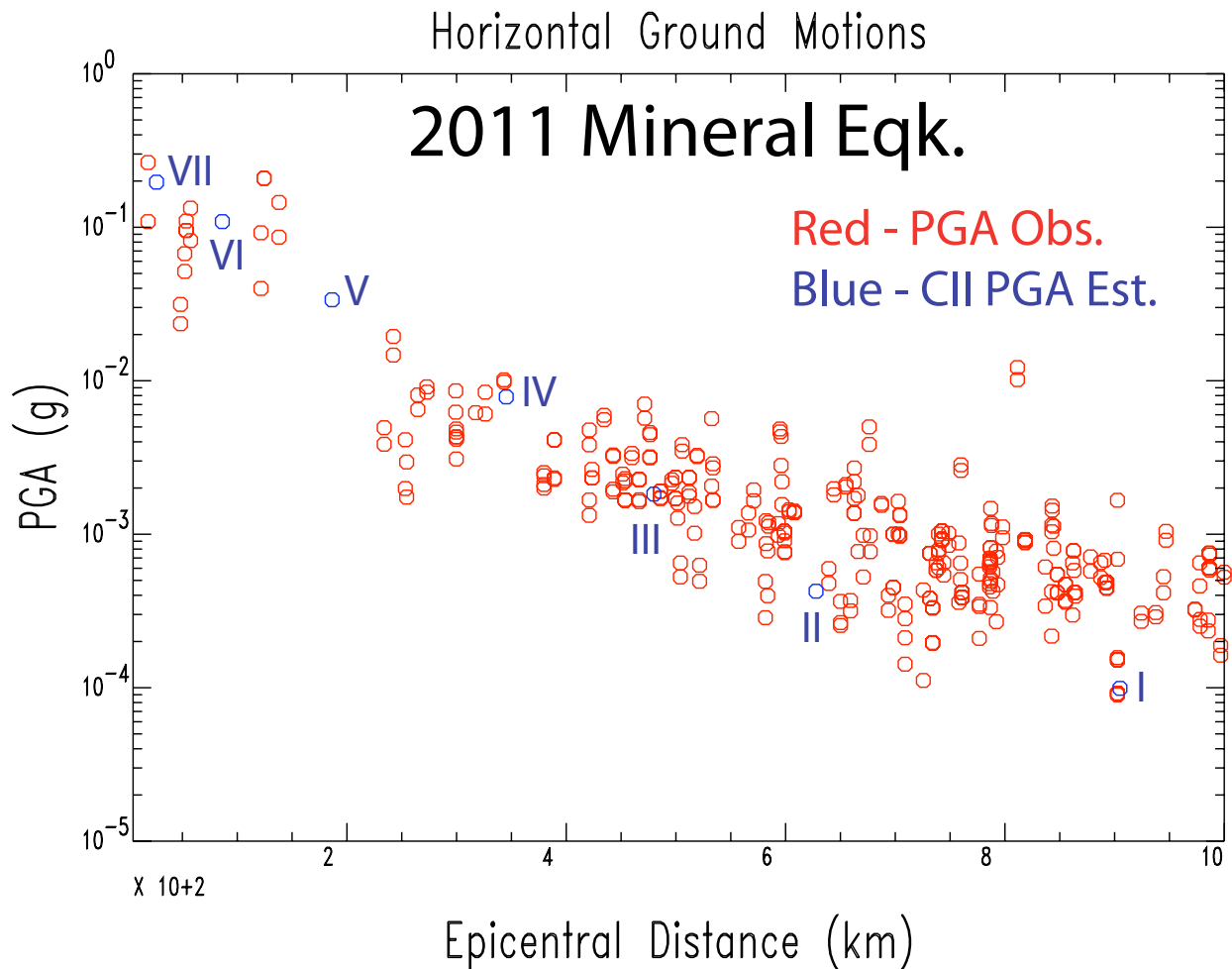


Figure 5: Observations for peak ground acceleration (PGA) from the 2011 M5.7 Mineral, VA earthquake (red circles) and estimates of ground motion from intensity (blue circles) by the method described in the text. The MMI level used for each estimate is also shown.

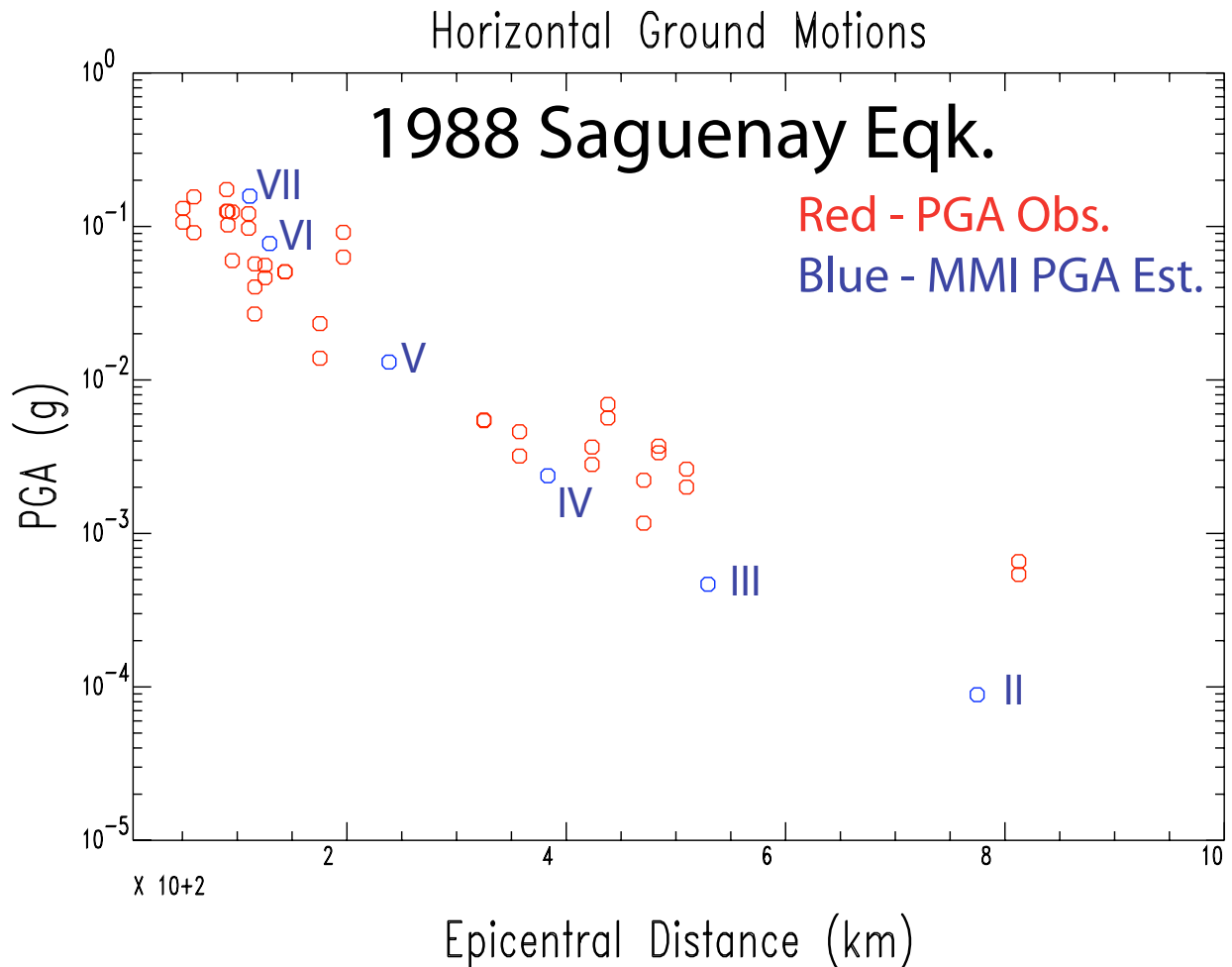


Figure 6: Similar plot for the 1988 M5.9 Saguenay, Quebec earthquake as Figure 5.

To make the historical earthquake estimates of ground motion from intensity observations usable in GMPE development, we need a reasonable estimate of the moment magnitudes of the historical events. Cramer and Boyd (2014) provide estimates for the three New Madrid mainshocks of 1811-1812 and the 1886 Charleston, SC earthquake of M7.5 (Dec. 16, 1811), M7.3 (Jan. 23, 1812), M7.7 (Feb. 7, 1812), and M7.0 (1886) with a 95% confidence limit uncertainty of ± 0.3 magnitude units. The 1925 Charlevoix, 1929 Grand Banks, and 1988 Saguenay earthquakes have published instrumental magnitudes of M6.2 (Bent, 1992), M7.2 (Bent, 1995), and M5.9 (GSC), respectively. Using the mean intensity at large distances approach of Cramer and Boyd (2014) and the 1925 M6.2 Charlevoix and 1988 M5.9 Saguenay earthquakes as reference earthquakes (MMI datasets of Cajka, 1999, and Cajka and Drysdale, 1996, respectively), we estimated a moment magnitude of M6.0 with a 95% confidence limit of ± 0.4 magnitude units for both the 1843 Marked Tree, AR and the 1870 Charlevoix, QC earthquakes using the MMI datasets of Bakun et al. (2002a) and Ebel et al. (2013), respectively. For the 1870 Charlevoix earthquake Ebel et al. (2013) estimated a moment magnitude of 5.8 ± 0.3 . After reevaluating the intensity values for the 1843 Marked Tree earthquake, Hough (2013) estimated the magnitude as M5.4 (no uncertainty estimated), but she stated that the lower magnitude is entirely related to the her intensity reevaluation. Hough's intensity assignment method is different from traditional historical MMI assignments, hers tending to be lower in

MMI, which makes a direct comparison of her magnitude estimate to ours based on the Bakun et al. (2002a) MMI assignments difficult. Obviously, we believe our estimate is better based on the magnitude estimation approach using mean intensity at large distances and an MMI assignment for the 1843 event consistent with the MMI assignments of the reference earthquakes. We were unable to estimate a moment magnitude for the 1895 M6+ Charleston, MO earthquake due to problems with the available MMI dataset (Bakun et al., 2002a). The problems include amplification in river valleys, a lower cut-off of III for MMI in historical observations, and a possible arbitrary truncation of observations with distance (Bakun et al., 2003).

MMI datasets for historic earthquakes used for estimating ground motions from intensities in this study are the 1811-1812 New Madrid and 1886 Charleston, SC assignments by Bakun et al. (2002b), the 1925 Charlevoix assignments by Cajka (1999), and the 1929 Grand Banks assignments by Bakun et al. (2002a). These magnitude assignments are traditional MMI assignments and were used to maintain a uniform intensity assignment approach in the analysis. As pointed out above, for our updates to Dangkua and Cramer (2011), we corrected more recent Community Internet Intensity (CII) values to traditional MMI values to again maintain a uniform approach in intensity assignments. The 1811-1812 New Madrid intensity datasets were reviewed for obvious outliers with distance and the outliers checked against Moran (2014; oral communication). Generally, the New Madrid intensity outliers were found to be false data points and removed for our analysis.

Figure 7 presents the median estimated PGA versus median distance curves for most of the historical M6 and M7 earthquakes plus the 1988 M5.9 Saguenay and 2011 M5.7 Mineral earthquakes for reference. The M6.0 1843 and 1870 earthquake estimated median PGA curves are not included because they do not have magnitudes significantly higher than the more recent M5.6-5.9 events with plentiful actual ground motion observations. The distribution of estimated PGA with distance and magnitude looks reasonable, with three exceptions: (1) the off-shore 1929 M7.2 Grand Banks earthquake's estimated median PGAs within a 1100 km median distance are biased to larger distances by missing intensity observations at closer-in distances, (2) the observed ground motion directivity for the 2011 M5.7 Mineral, VA earthquake is reflected in the intensity based estimates by the curve crossing the 1988 M5.9 Saguenay curve within a median distance of 200 km, and (3) the 1811 M7.5 New Madrid curve crosses below the 1886 M7.0 Charleston curve at median distances less than 600 km. The Saguenay actual ground motion observations also show directivity effects, but there are few Saguenay intensity observations in the direction of the directivity unlike the Mineral intensity observations. Thus the Mineral earthquake curve shows the effect of directivity and the Saguenay curve does not. The December 1811 M7.5 New Madrid earthquake has many more intensity observations within the Mississippi embayment than the other two New Madrid mainshocks, which have very few observations within the embayment. Thus the December 1811 curve possibly shows the effect of strong soil nonlinearity within the Mississippi embayment at strong ground motion levels.

Based on Figure 7 we have selected the intensity datasets to use in GMPE development as shown in Figure 8. The M7.2 Grand Banks earthquake curve has been restricted to median distances from MMI III and IV. The 1988 Saguenay and 2011 Mineral intensity datasets are not selected because they have plentiful actual ground motion observations. And the MMI II median distance

estimate for the 1925 Charlevoix earthquake is not shown due to poor sampling in distance biasing the median distance estimate.

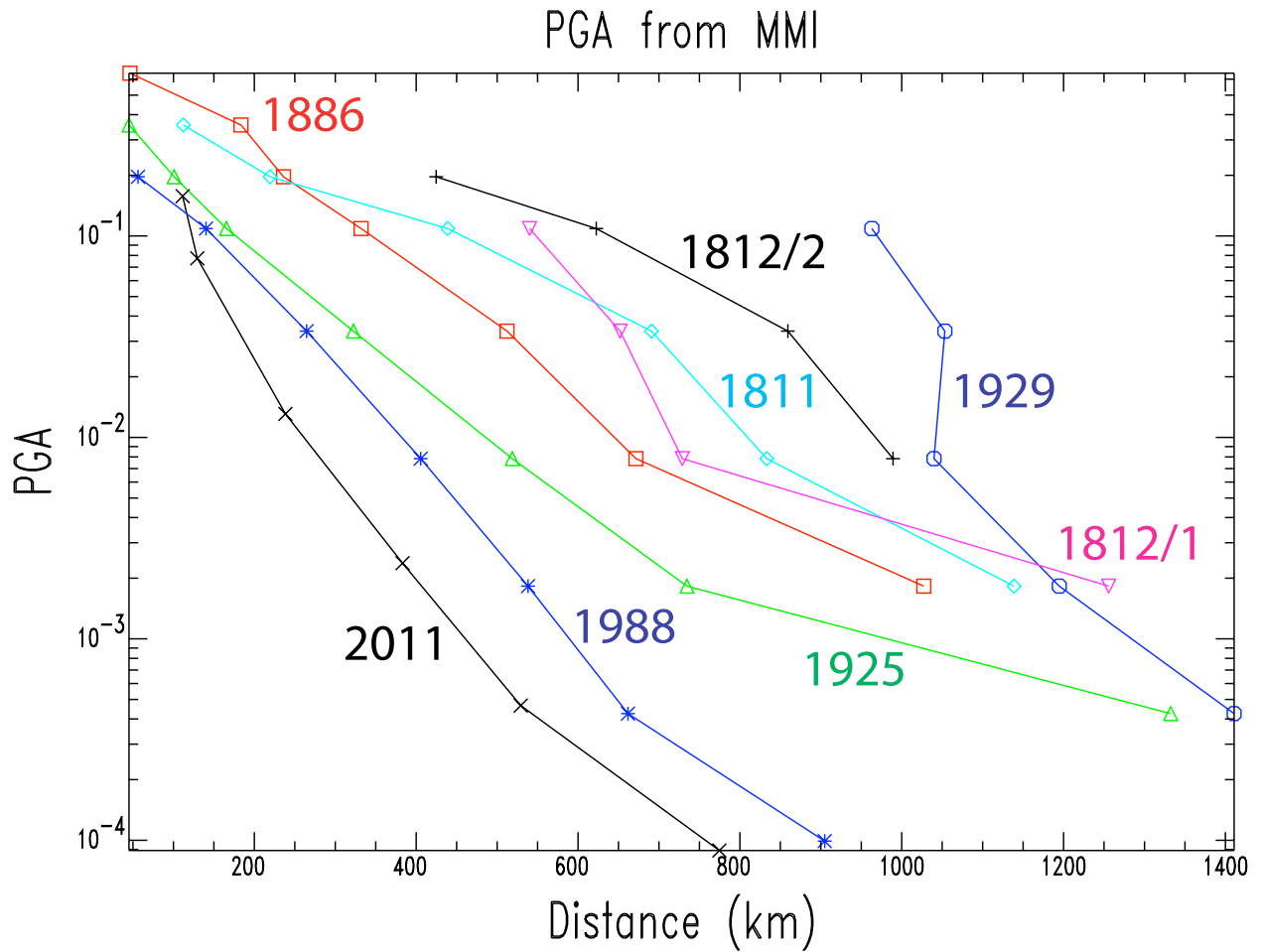


Figure 7: Median estimated PGA versus median distance from intensity curves for eight earthquakes. 1811 – M7.5 New Madrid, 1812/1 – M7.3 New Madrid, 1812/2 – M7.7 New Madrid, 1886 – M7.0 Charleston, SC, 1925 – M6.2 Charlevoix, 1929 – Grand Banks, 1988 – M5.9 Saguenay, and 2011 – M5.7 Mineral, VA earthquakes.

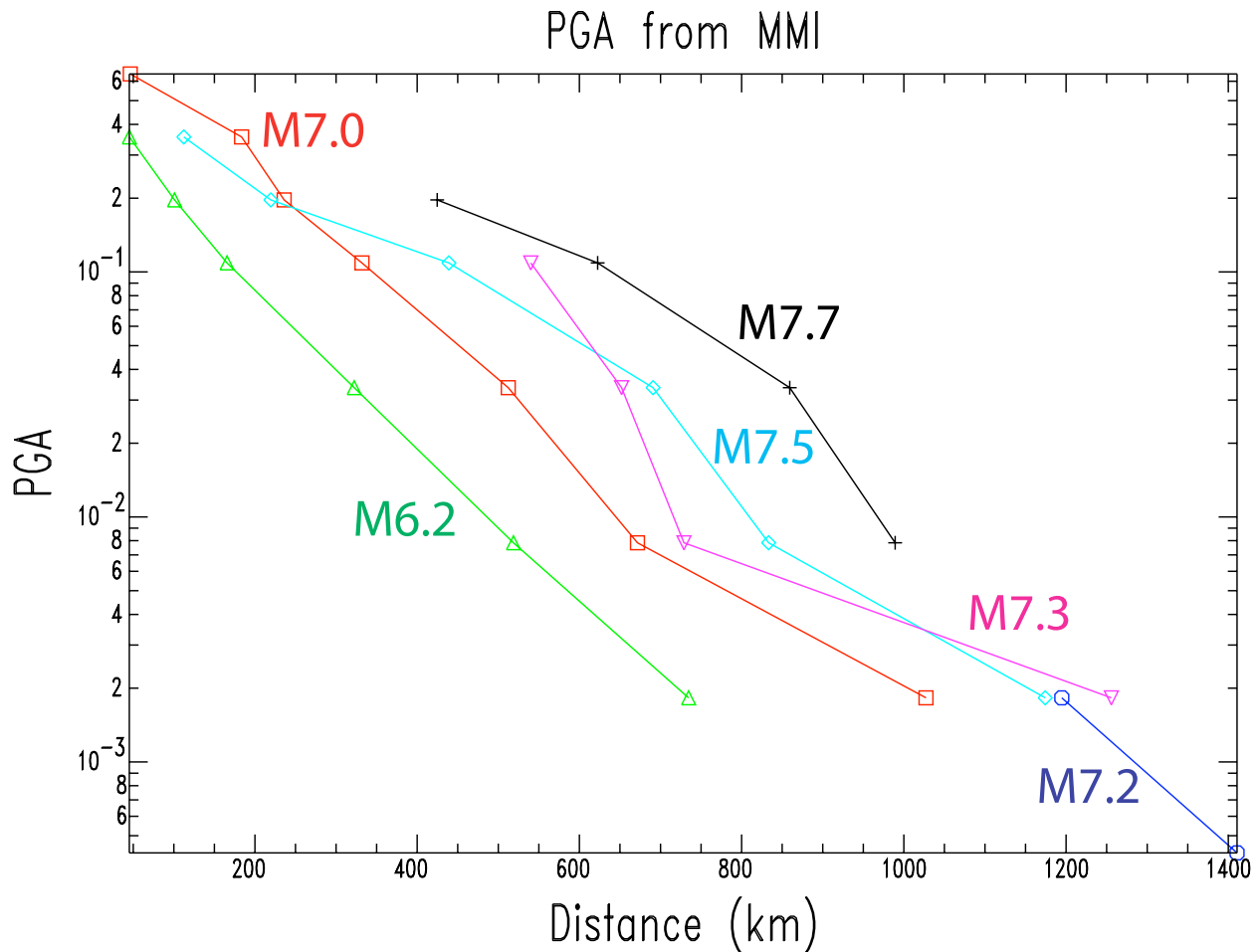


Figure 8: Historical earthquake curves selected from Figure 7 for used in the empirical GMPE regressions with intensity-based estimates of ground motion. M7.7 – Feb. 1812 New Madrid, M7.5 – Dec. 1811 New Madrid, M7.3 – Jan. 1812 New Madrid, M7.2 – 1929 Grand Banks, M7.0 – 1886 Charleston, SC, and M6.2 – 1925 Charlevoix earthquakes.

Figures 9 and 10 present both the median estimated PGA versus median distance curve and all the estimated PGAs from individual MMI observations for the 1811 M7.5 New Madrid and 1925 M6.2 Charlevoix earthquakes, respectively. The median curve and the individual estimates are alternative ways of incorporating the intensity data into the empirical GMPE regressions. By using estimated ground motions from the individual intensity observations we can carry uncertainty into the GMPE regressions and also obtain estimated ground motions at the more important closer-in distances, which is an advantage over the median curves. We have chosen to incorporate the selected intensity observations into the GMPE regressions using the individual observations, which also allows us to assign V_{s30} estimates based on the location of the intensity observation instead of assigning some sort of median V_{s30} estimates to the median curves.

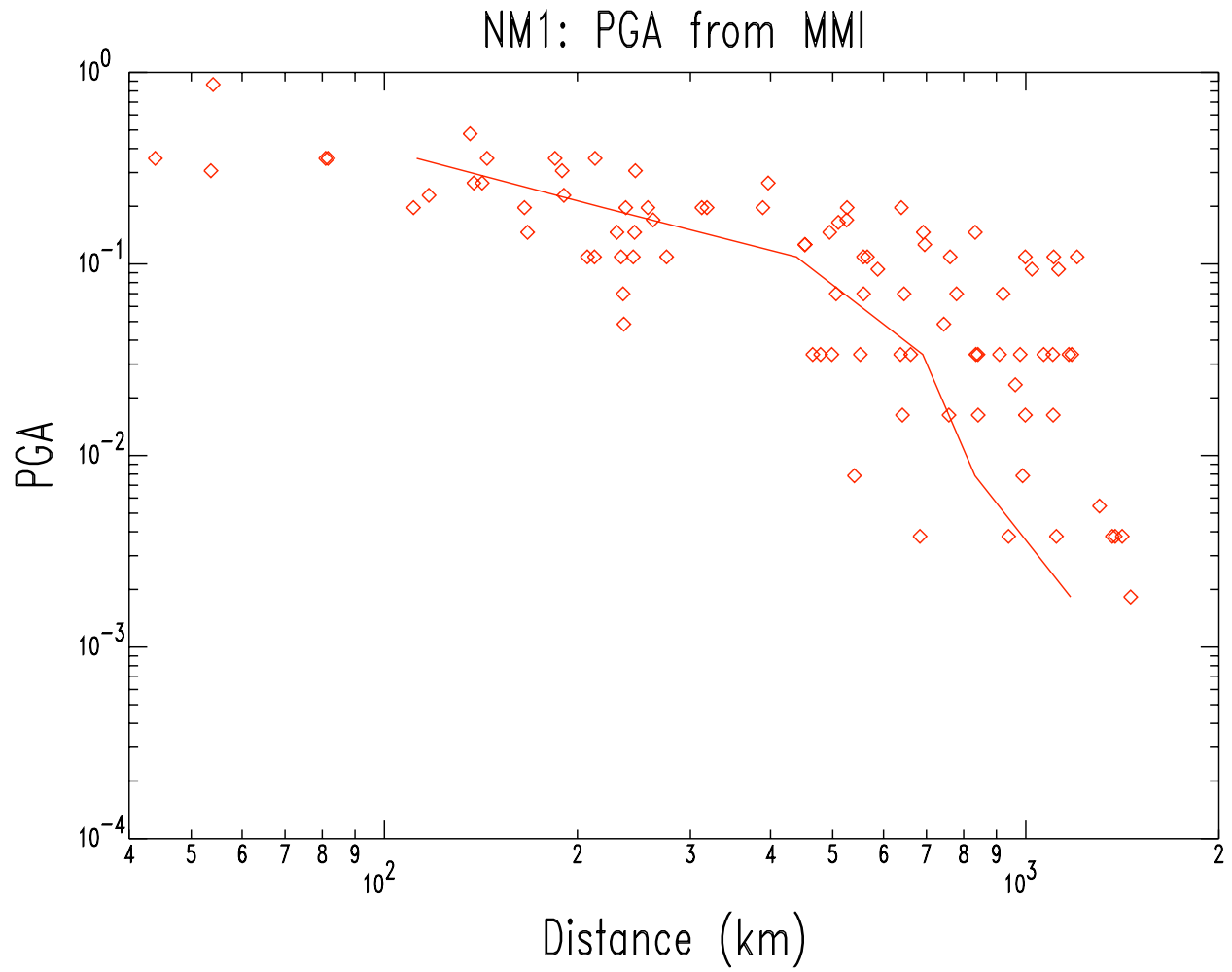


Figure 9: Median curve and individual intensity observations converted to PGA for the 1811 M7.5 New Madrid (NM1) earthquake.

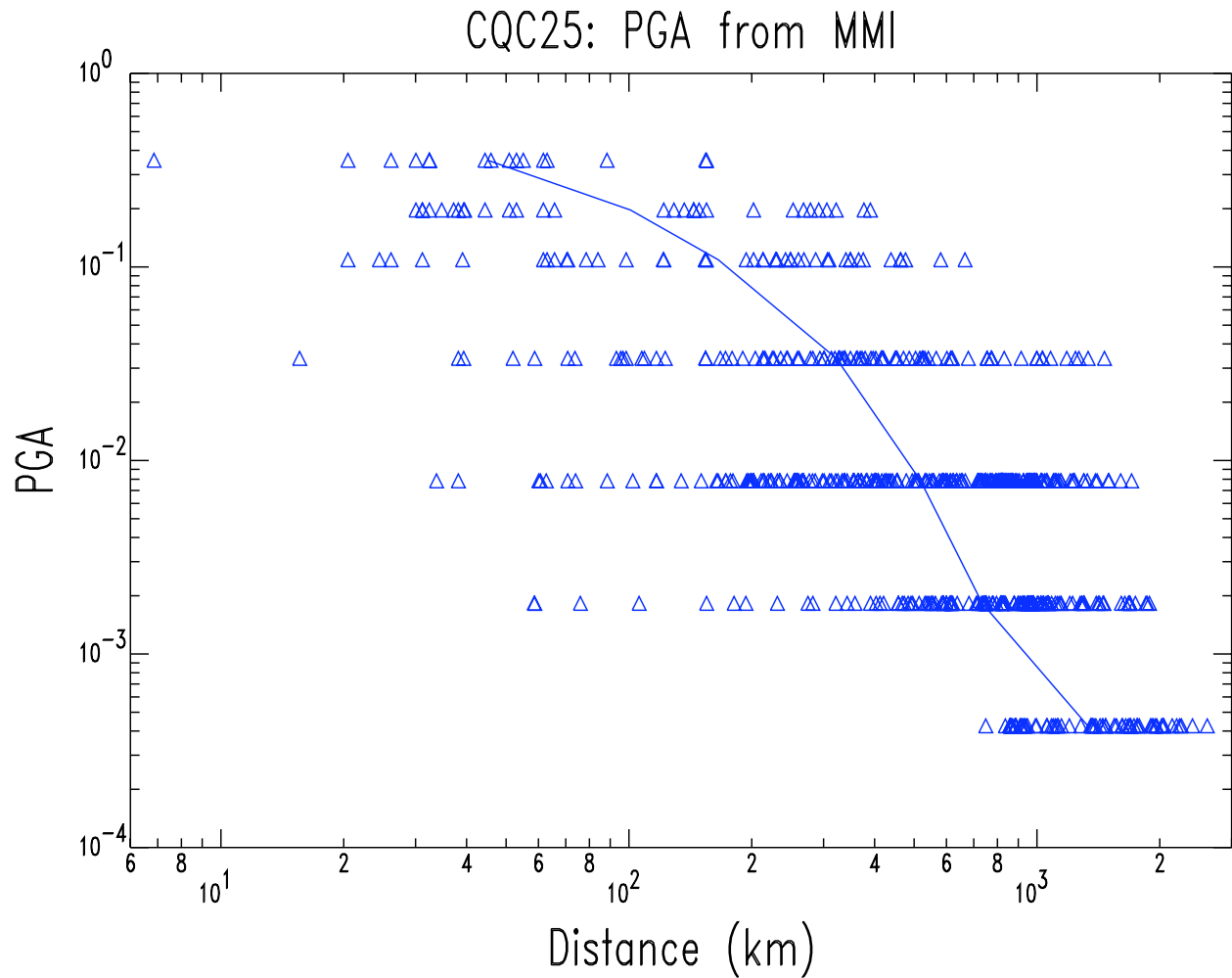
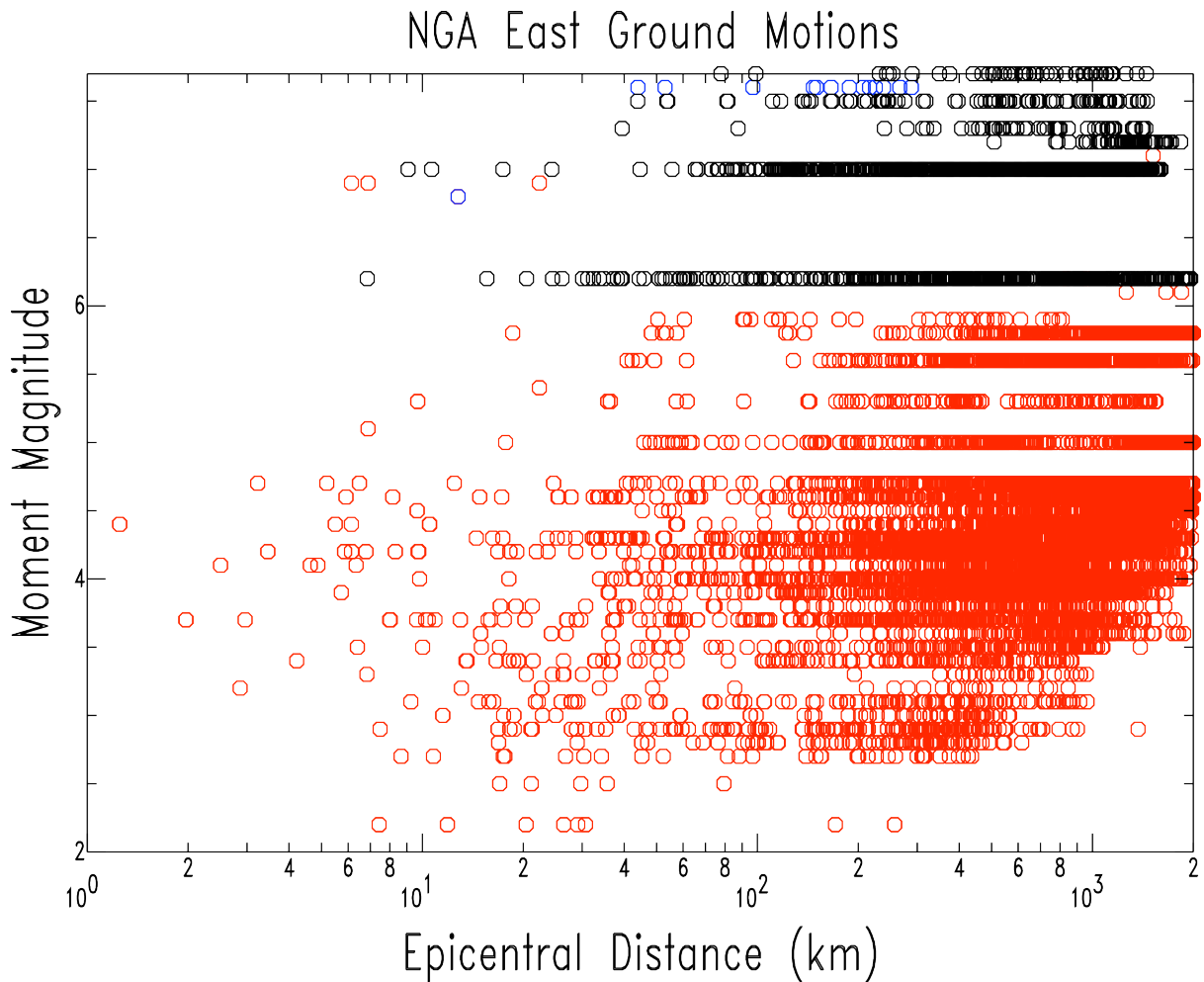


Figure 10: Median curve and individual intensity observations converted to PGA for the 1925 M76.2 Charlevoix (CQC25) earthquake.

Figure 11 presents a magnitude versus distance plot similar to Figure 1 with the selected intensity data added to the NGA East database. There are 1921 intensity observations that can be converted to ground motion estimates using intensity versus ground motion relations. Clearly the intensity data can add significantly to the $M > 6.0$ observations for distances as close as 10 km.



Blue - Bhuj, Gazli
Red - ENA
 Black - Intensity Based (1921 obs.)

Figure 11: NGA East with historical intensity distance vs. magnitude plot for all observations. Red circles are for ENA observations, blue circles are for Bhuj, India and Gazli, USSR observations, and black are for ENA intensity observations.

Vs30 Assignments

The form used in the GMPE regression has a Vs30 term (shown above), which requires an assignment of Vs30 for each observation. For NGA East data, Vs30 assignments were taken from the NGA East GMRotD50 flatfile (Spring 2014 beta version), which were developed by the NGA East project. For the intensity data, Vs30 was assigned for each intensity observation point using the Wald and Allen (2007) approach via the USGS Global Vs30 Map Server at <http://earthquake.usgs.gov/hazards/apps/vs30/>. Vs30 for the Gazli ground motion observation was provided by Vladimir Grazier (written communication). And Vs30 for the Bhuj ground motion observations has been assigned using the geology assignments in Cramer and Kumar (2003). For the latter, the geology assignments were simply Quaternary, Tertiary, and Rock,

which were interpreted as NEHRP site class D, C, and B and given mid-point Vs30s for each class of 270, 560, and 1130 m/s, respectively. One Bhuj site (Kandla) could be on either Quaternary or Tertiary deposits and so was given a Vs30 estimate corresponding to the C/D boundary value of 360 m/s.

Regression Results

The empirical GMPE regressions were performed both with and without the intensity-based ground motion estimates. This allowed us to evaluate the difference the intensity-based data makes in the regressions. The site condition reference for the regressions in this study is B/C boundary – Vs30 of 760 m/s. For these comparisons we have used the Dangkua and Cramer (2011) relations to convert the intensity observations to selected ground motions. These conversions are sufficient to gain insight into the impact of adding intensity-based ground motion estimates in the empirical GMPE regressions, which is a major goal of this research.

Figure 12 presents the M5.9 PGA regression results using the intensity and ground motion data. Also shown are the observations (corrected for the site term from the regression) for the 2011 M5.7 Mineral, VA, 1988 M5.9 Saguenay, QC, and 1925 M6.2 Charlevoix earthquakes. The 1925 observations are intensity based and the 1988 and 2011 observations are actual ground motions. The 1988 and 2011 data are fit well by the regression beyond 200 km and show known directivity effects in the ground motion observations (higher than predicted) for these two events at distances less than 200 km. The M6.2 1925 data are also fit well allowing for the increased magnitude level, but the scatter about the regression curve in the 1925 observations is significantly larger than the scatter in the 1988 and 2011 data, as expected for the intensity-based ground motion estimates.

Table 1 shows the impact on PGA variability of including the intensity observations in the regressions. The comparison is between regressions with and without the intensity data for within-event, between-event, and total variability. The Dangkua and Cramer (2011) intensity versus ground motion relations are used and the comparisons in the table are for PGA, PGV, 0.3s Sa, and 1.0s Sa. Clearly the added variability of the intensity data affects within-event variability more than between-event variability and hence the total aleatory variability. The added variability in the intensity data increases the within-event variability 20-30%, nominally does not change the between-event variability within 3-4% except for 1.0s Sa which increases ~16%, and only increases the total aleatory variability by 11-14% for PGA.

Table 1: Variability Comparisons between w/o and w/ intensity regressions (logarithm base 10).

Period	Within Event		Between Event		Total Variability	
	w/o MMI	w/ MMI	w/o MMI	w/ MMI	w/o MMI	w/ MMI
PGA	0.32	0.38	0.31	0.30	0.44	0.49
PGV	0.30	0.36	0.30	0.31	0.42	0.48
0.3 s	0.32	0.41	0.30	0.29	0.44	0.50
1.0 s	0.31	0.39	0.25	0.29	0.40	0.49

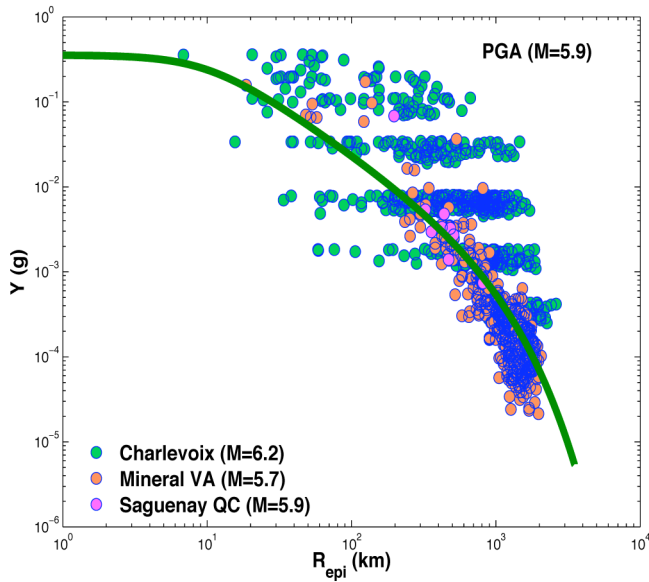


Figure 12: Mean PGA GMPE curve with intensity observations for M5.9.

To visualize the difference in the regressions with and without the intensity data, we plotted these regressions along with neighboring observations (again corrected for the site term from the regression) for M5.7, near the upper end of the NGA East magnitude range of plentiful ground motion observations, and for M7.6, where actual ground motion observations are very few and estimates from intensity have their greatest impact. Figure 13 shows this comparison for PGA. Both regressions fit the observations well beyond 100 km, with the regression with the intensity data lowering the predicted ground motions (not always dramatically) at distances less than 100 km, where data observations are still sparse near these magnitude levels and nonexistent at less than 20-40 km. The addition of the intensity data to the regression has little effect at the M5.7 level, but for M7.6 lowers ground motion predictions by a factor of about 2 at distances less than 100 km. The presence of the Bhuj PGA observations helps the w/o intensities regression not to be dramatically different from the w/ intensities regression.

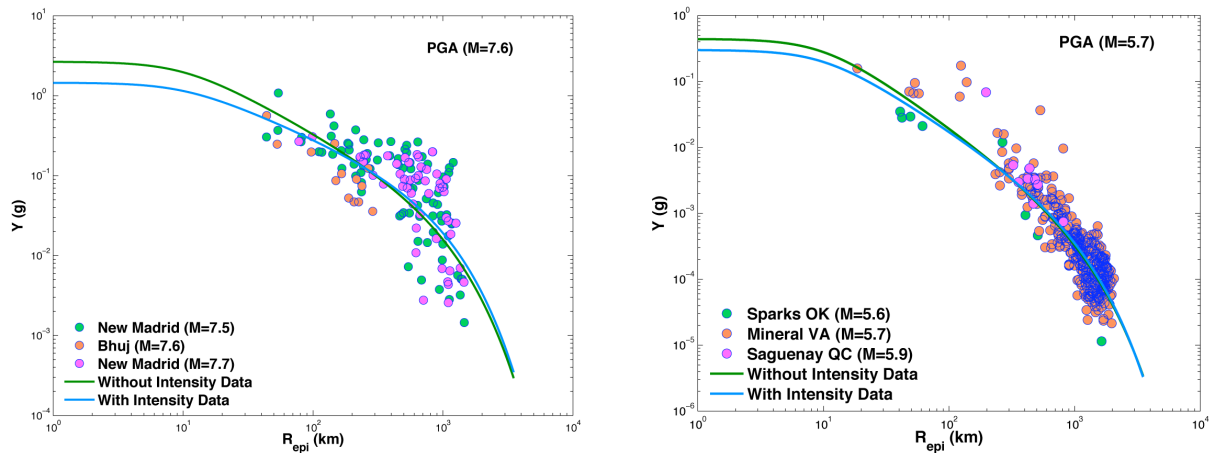


Figure 13: PGA with and without intensity regression comparisons with near magnitude observations for M7.6 (left) and M5.7 (right).

Figure 14 shows for 0.3s Sa a similar comparison to Figure 13 for PGA. At 0.3 s both regressions are very similar, with the M7.6 w/intensities regression only slightly lowering the ground motion predictions. Note that there is no Bhuj 0.3 s Sa observations to help constrain the w/o intensities regression but there are a few high M6 observations close-in from Nahanni and Gazli.

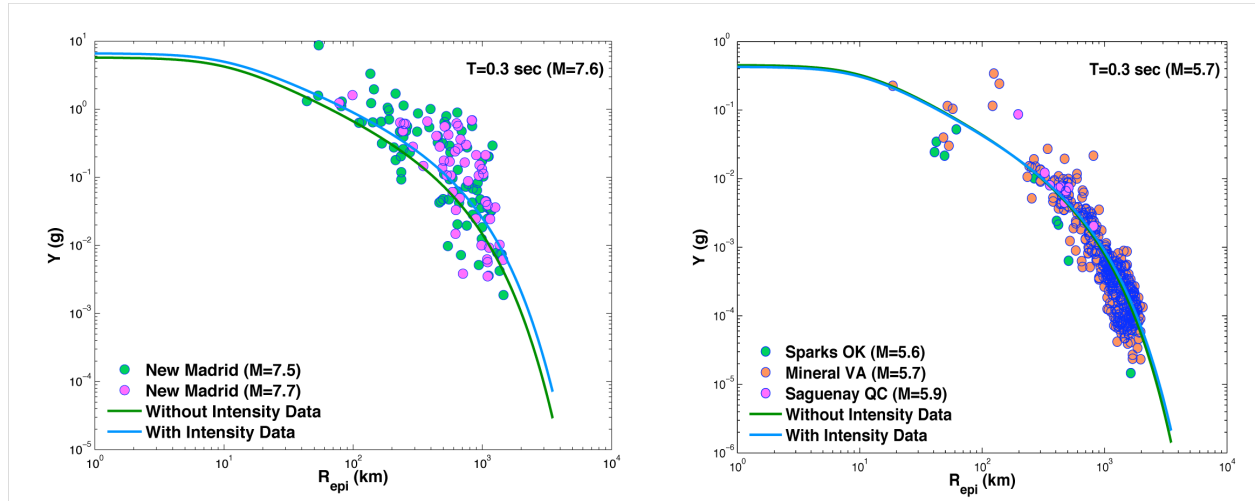


Figure 14: 0.3 s Sa with and without intensity regression comparisons with near magnitude observations for M7.6 (left) and M5.7 (right).

Figure 15 shows the regression comparison for PGV. For M5.7, the w/intensity regression predicts lower ground motions by a factor of 1.3 to 2 and better fits the lower Brune stress-drop (~100 bars) Sparks, OK earthquake observations. The higher Brune stress-drop (~200 and ~400 bars, respectively) Mineral, VA and Saguenay, QC earthquake observations with directivity effects within 200 km fall above the w/intensity prediction and are better fit by the w/o intensity regression beyond 200 km. For M7.6, the w/intensity regression dramatically lowers the ground motion predictions by factor of 10. Due to Dangkua and Cramer's (2011) ENA PGV relation not having observations above MMI VI and being significantly different than their California PGV relation, the intensity observations above MMI VI are not shown in Figure 15 and not included in this w/intensities regression. The updated relations, presented in the Appendix, do extend the ENA PGA relation above MMI VI because of added observations and hence should better constrain w/intensities empirical regressions.

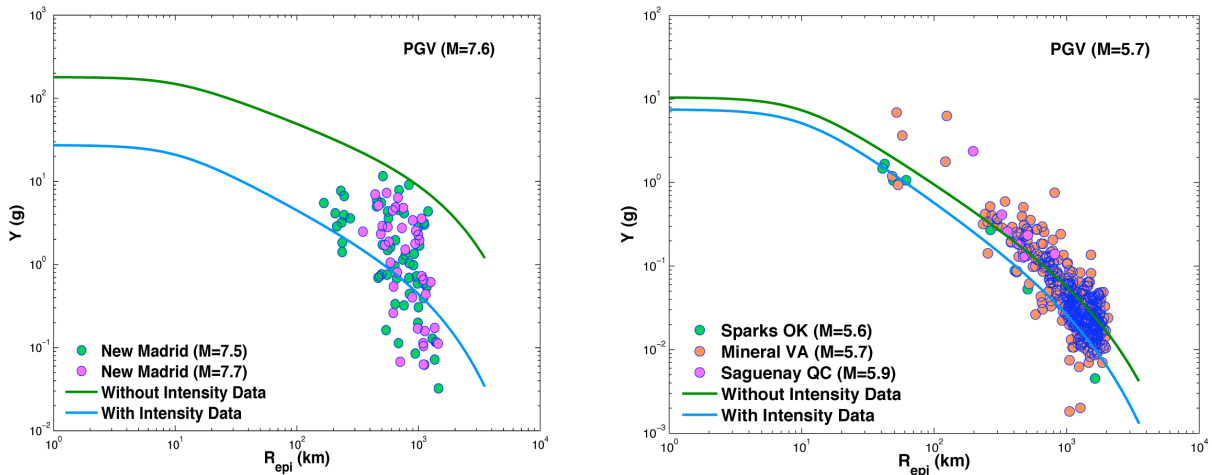


Figure 15: PGV with and without intensity regression comparisons with near magnitude observations for M7.6 (left) and M5.7 (right).

Finally, Figure 16 shows the comparison for 1.0s Sa. For M5.7, the w/intensity regression predicts lower ground motions beyond 500 km and higher ground motions closer than 500 km, by up to a factor of 2. For M7.6, the w/intensity regression predicts lower ground motions by a factor of 10, except within 100 km where the Bhuj observations pull the w/intensity regression higher. Again, the observations for MMI VII and VIII are not available for the regression due to the same limitations for the Dangkua and Cramer (2011) 1.0 s Sa relations as for their PGV relations. Also the Bhuj 1.0 s Sa observations may better follow the Brune source spectrum model (Brune, 1970, 1971) as shown by Bodin et al. (2004) for Bhuj aftershocks up to M5. If this is the case, the Bhuj 1.0 s Sa observations maybe higher than expected for ENA where intermediate spectral sag (Atkinson, 1993) has been observed for large earthquakes. Thus the inclusion of the Bhuj 1.0 s Sa observations in the regressions may inappropriately bias the results at 1.0 s.

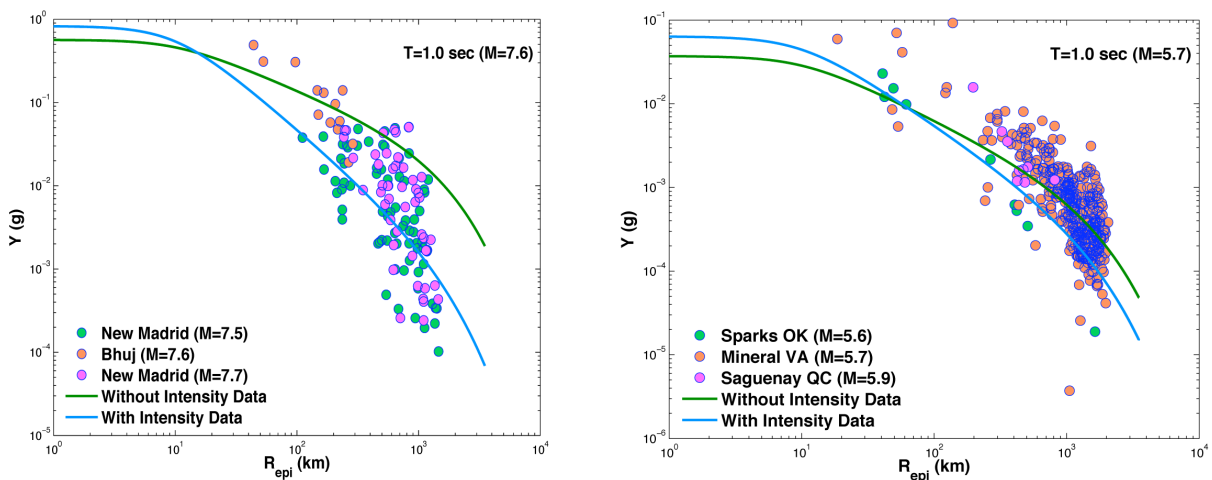


Figure 16: 1.0 s Sa with and without intensity regression comparisons with near magnitude observations for M7.6 (left) and M5.7 (right).

Conclusions

Combining intensity-based estimates of ground motion with the NGA East ground motion database provides observational coverage from M2.5 to M7.7 over a distance range of less than 10 km to 2000 km. The intensity-based estimates help constrain empirical ENA GMPEs at $M \geq 6$, although with greater uncertainty. But there are still not empirical constraints at distances less than 20-40 km for magnitudes greater than M6.0. It is also possible that the limited long-period observations from the 2001 M7.6 Bhuj earthquake inappropriately bias empirical regressions because they are well fit by the Brune source model without the intermediate spectral sag observed in ENA large earthquakes.

Acknowledgements

Figures in this report were generated using GMT (Wessel and Smith, 1991) and SAC (Goldstein et al., 2003).

References

- Al Noman, M.N. (2013). *Ground motion modeling for eastern North America: an empirical approach with the NGA-East database*, M.S. thesis, University of Memphis, Memphis, TN, 54 pp.
- Atkinson, G.M. (1993). Earthquake source spectra in eastern North America, *Bull. Seism. Soc. Am.* **83**, 1778-1798.
- Atkinson, G.M., and D.J. Wald (2007). "Did you feel it?" intensity data: a surprisingly good measure of earthquake ground motion, *Seism. Res. Lett.* **78**, 362–368.
- Bakun, W.H. and C.M. Wentworth (1997). Estimating earthquake location and magnitude from seismic intensity data, *Bull. Seism. Soc. Am.* **87**, 1502-1521.
- Bakun, W.H. and M.G. Hopper (2004). Magnitudes and locations of the 1811–1812 New Madrid, Missouri, and the 1886 Charleston, South Carolina, Earthquakes, *Bull. Seism. Soc. Am.* **94**, 64–75.
- Bakun, W.H., A.C. Johnston, and M.G. Hopper (2002a). *Modified Mercalli intensities (MMI) for some earthquakes in Eastern North America (ENA) and empirical MMI site corrections for Towns in ENA*, U.S. Geological Survey, Open-File Report 02-109, 72pp.
- Bakun, W.H., A.C. Johnston, and M.G. Hopper (2002b). *Modified Mercalli intensities (MMI) for large earthquakes near New Madrid, Missouri, in 1811–1812 and near Charleston, South Carolina, in 1886*, U.S. Geological Survey, Open-File Report 02-184, 31pp.
- Bakun, W.H., A.C. Johnston, and M.G. Hopper (2003). Estimating locations and magnitudes of earthquakes in eastern North America from modified Mercalli intensities, *Bull. Seism. Soc. Am.* **93**, 190-202.

- Bent, A.L. (1992). A re-examination of the 1925 Charlevoix, Quebec, earthquake, *Bull. Seism. Soc. Am.* **82**, 2097-2113.
- Bent, A.L. (1995). A complex double-couple source mechanism for the Ms 7.2 1929 Grand Banks earthquake, *Bull. Seism. Soc. Am.* **85**, 1003-1020.
- Bodin, P., L. Malagnini, and A. Akinci (2004). Ground-motion scaling in the Kachchh Basin, India, deduced from aftershocks of the 2001 Mw 7.6 Bhuj earthquake, *Bull. Seism. Soc. Am.* **94**, 1658–1669.
- Brune, J.N. (1970). Tectonic stress and spectra of seismic shear waves from earthquakes, *J. Geophys. Res.* **75**, 4997–5009.
- Brune, J.N. (1971). Correction (to Brune, 1970), *J. Geophys. Res.* **76**, 5002.
- Cajka, M.G. (1999). *The 1925 Charlevoix, Quebec, earthquake: reevaluation of the Canadian intensity data using the modified Mercali scale*, Geological Survey of Canada, Open File 3786, 79 pp.
- Cajka, M.G., and J.A. Drysdale (1996). *Intensity report of the November 25, 1988 Saguenay, Quebec, earthquake*, Geological Survey of Canada, Open File 3279, 71 pp.
- Cramer, C.H., and A. Kumar (2003). 2001 Bhuj, India earthquake engineering seismoscope recordings and eastern North America ground-motion attenuation relations, *Bull. Seism. Soc. Am.* **93**, 1390–1394.
- Cramer, C.H., and O.S. Boyd (2014). Why the New Madrid earthquakes are M7-8 and the Charleston earthquake is ~M7, *Bull. Seis. Soc. Am.* **104**, in press.
- Cramer, C.H., J. Kutliroff, and D. Dangkoa (2009). *Second year final report on a database of CEUS ground motions*, cooperative agreement: 07CRAG0015-Mod1, Final Report to the USGS, July 22, 2009, CERI, 12 pp, <https://umdrive.memphis.edu/ccramer/public/NGAeast/Documentaion/SecondYearFinalReportCEUSGMDatabase.doc>.
- Cramer, C.H., J.R. Kutliroff, and D.T. Dangkoa (2010). A database of eastern North America ground motions for the Next Generation Attenuation East project, Proceedings of the Ninth U.S. National and Tenth Canadian Conference on Earthquake Engineering: Reaching Beyond Borders, Earthquake Engineering Research Institute and Canadian Association for Earthquake Engineering, 10 p.
- Cramer, C.H., J.R. Kutliroff, and D.T. Dangkoa (2011). *Next Generation Attenuation East Initial Flat Files for Eastern North America*, Report to PEER accompanying NGA East flat files and time series under subagreement 7140, 4 pp.

- Dangkua, D.T., and C.H. Cramer (2011). Felt intensity vs. instrumental ground motion: a difference between California and eastern North America?, *Bull. Seism. Soc. Am.* **101**, 1847-1858.
- Ebel, J.E., M. Dupuy, and W.H. Bakun (2013). Assessing the location and magnitude of the 20 October 1870 Charlevoix, Quebec, earthquake, *Bull. Seis. Soc. Am.* **103**, 588-594.
- Goldstein, P., D. Dodge, M. Firpo, Lee Minner (2003). SAC2000: Signal processing and analysis tools for seismologists and engineers, Invited contribution to *The IASPEI International Handbook of Earthquake and Engineering Seismology*, Edited by WHK Lee, H. Kanamori, P.C. Jennings, and C. Kisslinger, Academic Press, London.
- Hough, S.E. (2013). Spatial variability of “Did You Feel It?” intensity data: insights in to sampling biases in historical earthquake intensity distributions, *Bull. Seism. Soc. Am.* **103**, 2767-2781.
- Hough, S.E. (2014). Earthquake intensity distributions: a new view (abstract), *Seism. Res. Ltrrs.* **85**, 526-527.
- Joyner, W.B., and D.M. Boore (1993). Methods for regression analysis of strong motion data, *Bull. Seism. Soc. Am.* **83**, 469-487.
- Joyner, W. B. and D. M. Boore (1994). Errata: Methods for regression analysis of strong-motion data, *Bull. Seism. Soc. Am.* 84.
- Moran, N.K. (2014). “The published accounts being few in number and incomplete in details,” a revision of the historic sources for the December 16, 1811 New Madrid earthquake, *Seism. Res. Ltrrs.*, submitted.
- Wald, D.J., and T.I. Allen (2007). Topographic slope as a proxy for seismic site conditions and amplification, *Bull. Seism. Soc. Am.* **97**, 1379-1395.
- Wessel, P. and W. H. F. Smith (1991). Free software helps map and display data, *EOS Trans. AGU* **72**, 441.

Publications from this Research

No publications have resulted from this research as of this date. Future papers based on this work will be provided, as required, when publication occurs.

Appendix

This appendix presents our update to the Dangkua and Cramer (2011) relations. The approach to updating the relations is discussed in the body of the report. This update is for GMRotD50 values, but other ground motion measures can easily be generated.

Table A1 shows the number of observations in each MMI bin after adjusting the CII values to MMI values using the approach suggested by Sue Hough (see body of the report). Decimal MMI values have been rounded for binning purposes. For longer periods the numbers in each MMI bin are reduced, except for MMI VII and VIII, because there are progressively fewer ground motion observations above the background noise at successively longer periods for smaller magnitude earthquake recordings. Currently there are no MMI IX observations in eastern North America (ENA) and only one MMI VIII observation. Also the distribution of MMI I observations with distance is insufficient due to incomplete assigning of MMI I in distance (due to assignment to higher MMI closer-in or truncating/missing data at greater distances). To avoid incomplete sampling issues, mean ground motions for MMIs I and VIII are not included in the regressions presented below. There are only five MMI VII observations, which maybe under sampling the range of ground motions observed for MMI VII. But retaining the mean ground motions for MMI VII in the regressions does not greatly alter the coefficients from regression without the MMI VII mean ground motion. Additionally, including the MMI VII value provides less variability among the period-dependent values for the coefficient associated with the dependent variable and the resulting linear regression curve has a more uniform relationship with the MMI VIII value (near or below the regression line). Thus the regressions with the MMI VII information are more consistent with the MMI VIII value (7.5) being rounded up from the lower limit of the MMI VIII bin range.

Table A1: Number of MMI observations in each MMI bin used in the regressions.

Bin:	I	II	III	IV	V	VI	VII	VIII
#:	81	195	228	124	95	20	5	1

Linear least-squares regression was performed with both MMI and median logGM (logarithm base 10 of ground motion) as the dependent variable. The forms of the regression are

$$\log GM = p_1 * MMI + p_2 \tag{A1}$$

and

$$MMI = q_1 * \log GM + q_2, \tag{A2}$$

where p_1 , p_2 and q_1 , q_2 are coefficient pairs from each regression. Equation A2 is the basic form used in Dangkua and Cramer (2011).

Table A2 presents the regression results with MMI and logGM as the dependent variable (Equations A1 and A2). Ground motion units are g except for PGV, which is cm/s. Note the stability of the dependent variable coefficients with period, suggesting that the relations maybe period independent for the dependent variable coefficient, within 10%.

Table A2: Regression coefficients for Equations A1 and A2.

	p ₁	p ₂	q ₁	q ₂
PGA	0.52027	-4.62349	1.91470	8.86984
PGV	0.50301	-2.92061	1.94036	5.77494
0.1s	0.54176	-4.45730	1.83943	8.21446
0.2s	0.50639	-4.28057	1.96125	8.42606
0.3s	0.49897	-4.32930	1.95901	8.58245
0.4s	0.48520	-4.39571	2.00474	8.93510
0.5s	0.47367	-4.46360	2.04220	9.26257
0.6s	0.47034	-4.57300	2.05275	9.54247
0.7s	0.47081	-4.68805	2.04780	9.76162
0.75s	0.46794	-4.73029	2.05959	9.90548
0.8s	0.46922	-4.78462	2.04682	9.97142
0.9s	0.46396	-4.85293	2.06680	10.21491
1.0s	0.54176	-4.45730	2.06083	10.37570
2.0s	0.48965	-5.64044	1.92418	11.11347
3.0s	0.51481	-6.05334	1.86073	11.45296
4.0s	0.52306	-6.31537	1.83169	11.75642
5.0s	0.52271	-6.51071	1.82017	12.06918
6.0s	0.52129	-6.67360	1.82588	12.40203
7.0s	0.52826	-6.84756	1.80174	12.55449
7.5s	0.53023	-6.92372	1.79590	12.64920
8.0s	0.53260	-6.99436	1.78733	12.71750
9.0s	0.53605	-7.12175	1.77607	12.86439
10.s	0.54042	-7.24048	1.76280	12.97660

Figures A1-A23 present the ENA MMI dependent regression results at each period plotted with the median logGM values and there 95% confidence estimates and the actual observations at MMI VII and VIII. Notice that within uncertainties, the linear trend of MMI VI and below appears to extend to MMI VII and possibly VIII in ENA. This is controlled mainly by observations from one earthquake (2011 M5.7 Mineral, VA earthquake) and thus may not be fully representative of the intensity versus ground motion relationship in ENA. However, the currently available data suggests that this linear (instead of the California bilinear) trend might be the case for ENA.

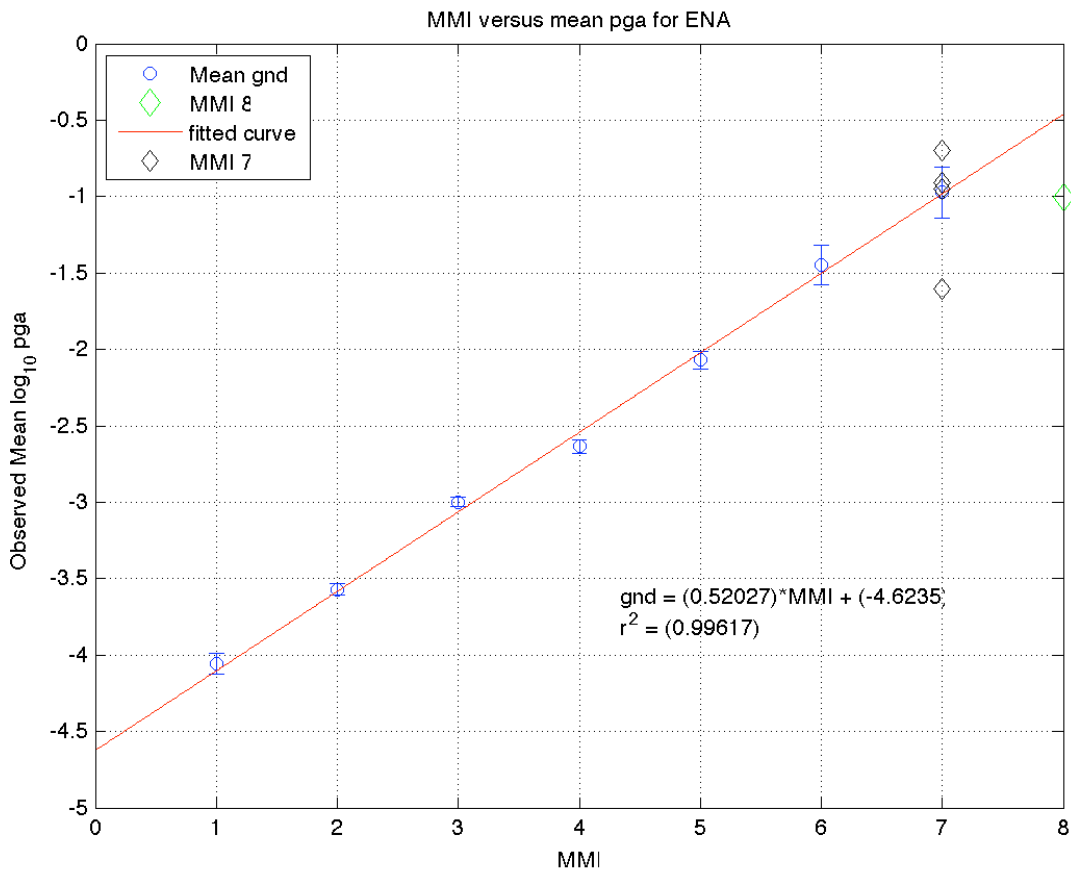


Figure A1: PGA regression for Equation A1 plotted with median logGM and its 95% confidence limits plus logGM values for MMI VII and VIII.

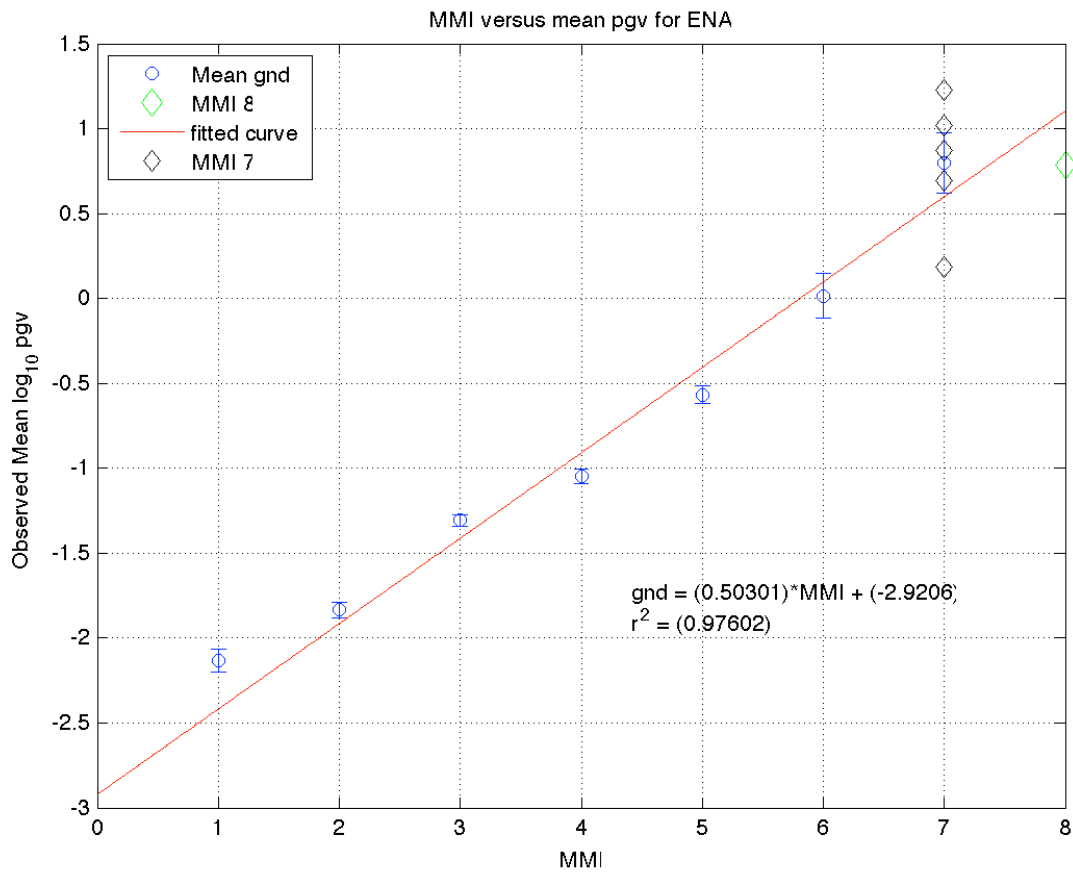


Figure A2: PGV regression for Equation A1 plotted with median logGM and its 95% confidence limits plus logGM values for MMI VII and VIII.

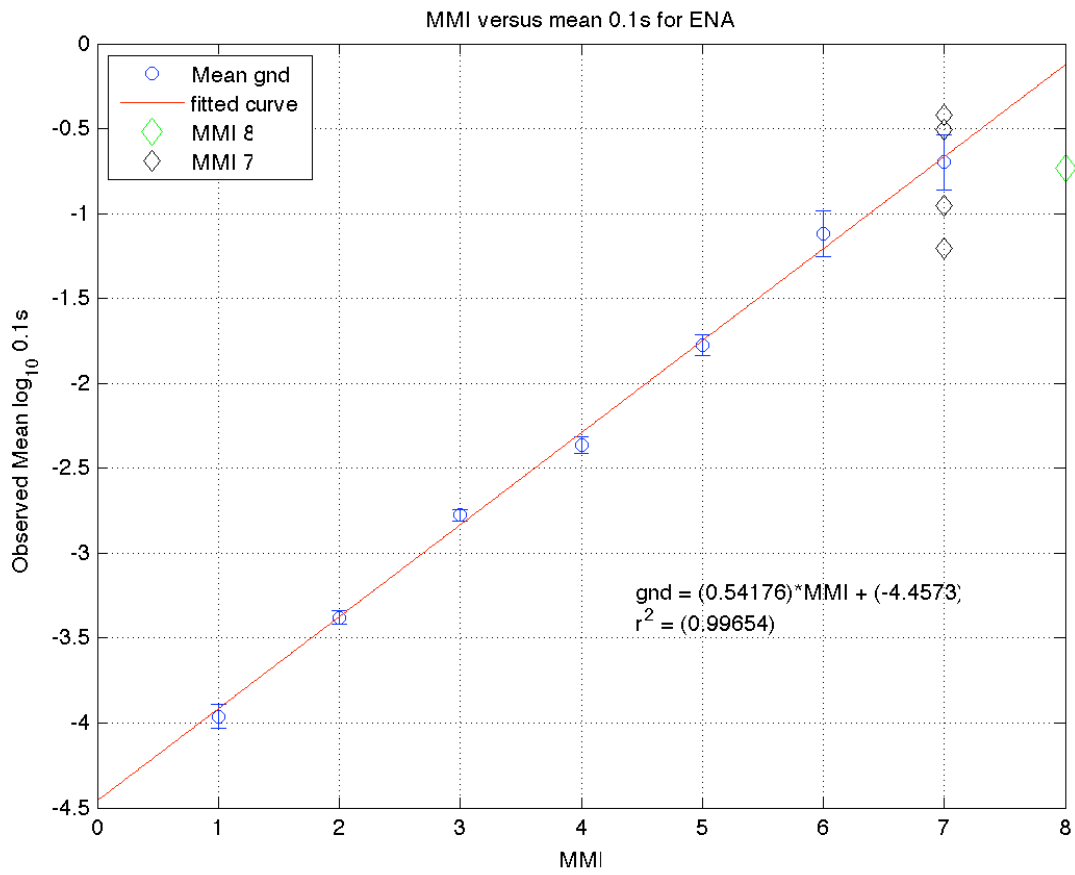


Figure A3: 0.1 s Sa regression for Equation A1 plotted with median logGM and its 95% confidence limits plus logGM values for MMI VII and VIII.

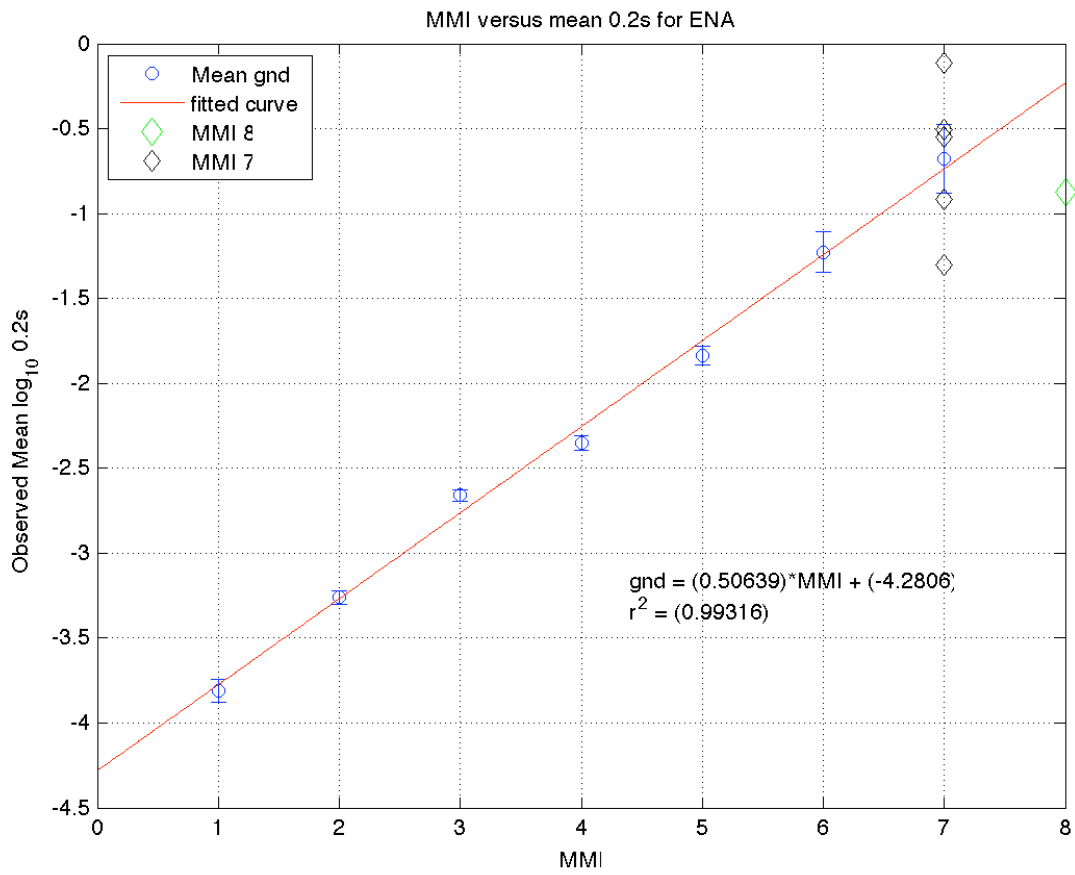


Figure A4: 0.2 s Sa regression for Equation A1 plotted with median logGM and its 95% confidence limits plus logGM values for MMI VII and VIII.

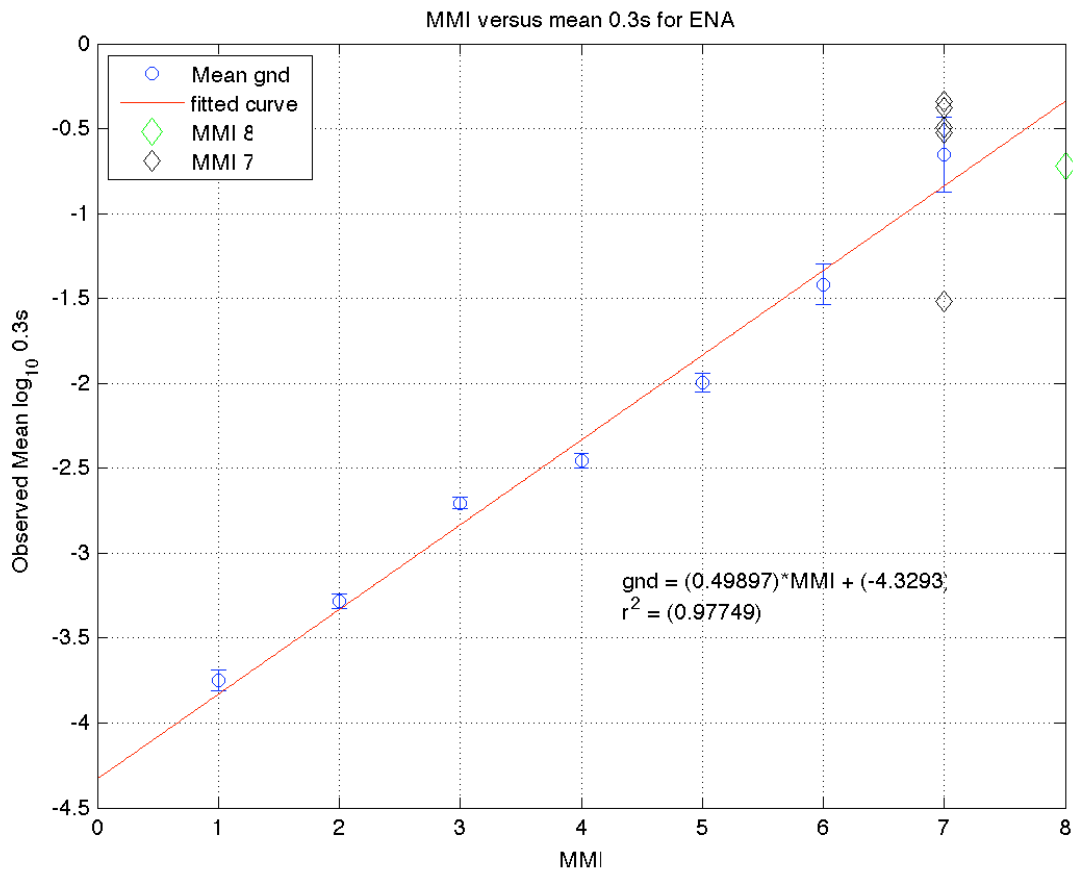


Figure A5: 0.3 s Sa regression for Equation A1 plotted with median logGM and its 95% confidence limits plus logGM values for MMI VII and VIII.

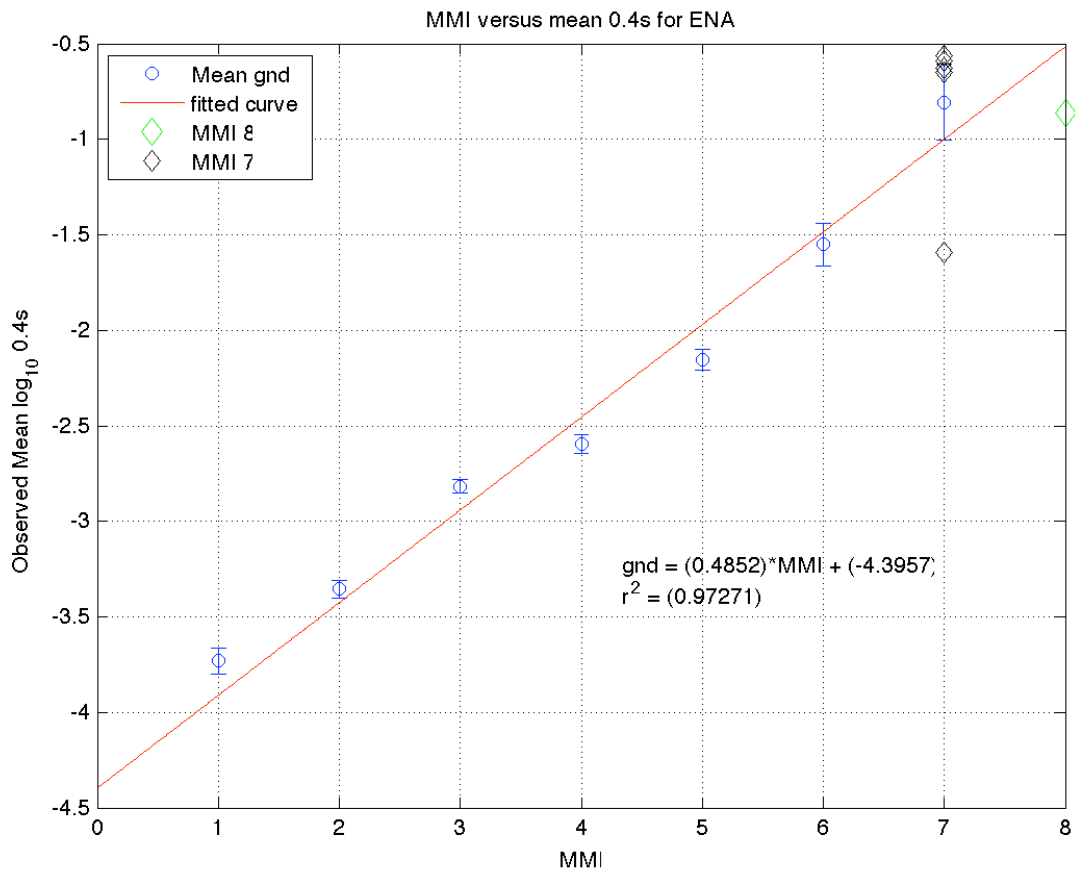


Figure A6: 0.4 s Sa regression for Equation A1 plotted with median logGM and its 95% confidence limits plus logGM values for MMI VII and VIII.

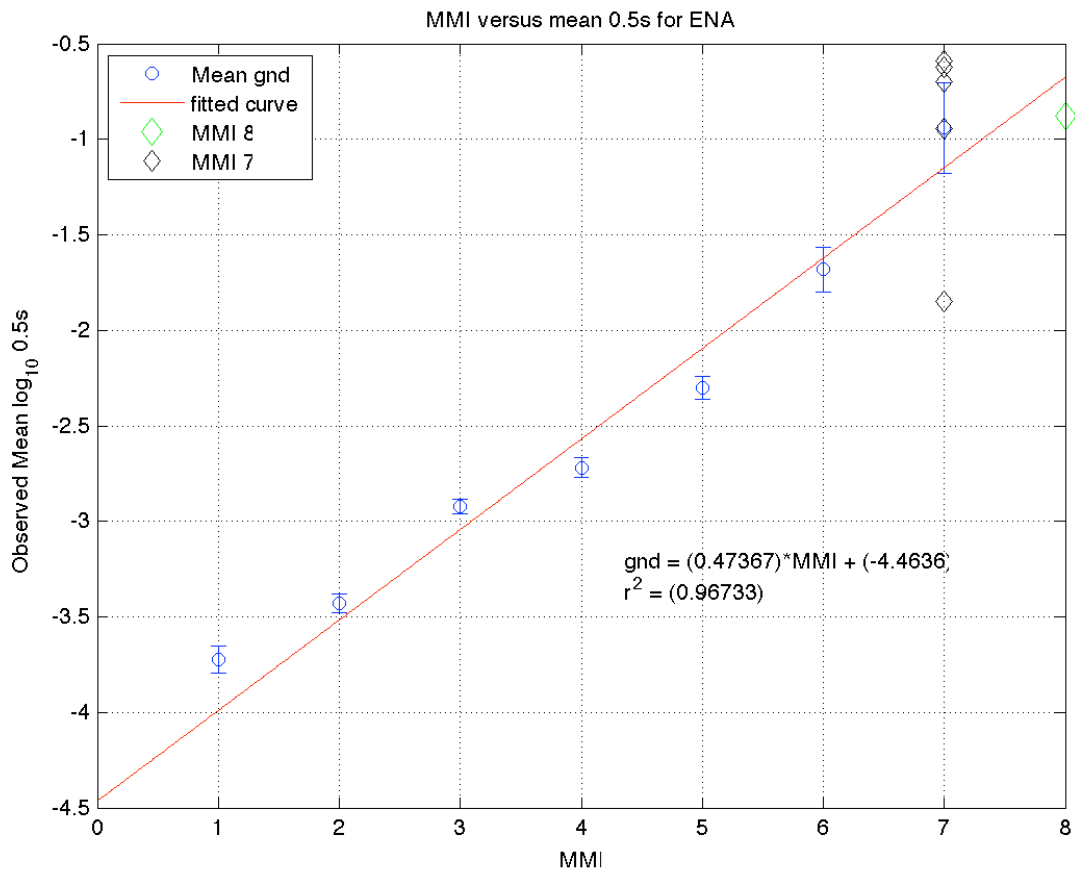


Figure A7: 0.5 s Sa regression for Equation A1 plotted with median logGM and its 95% confidence limits plus logGM values for MMI VII and VIII.

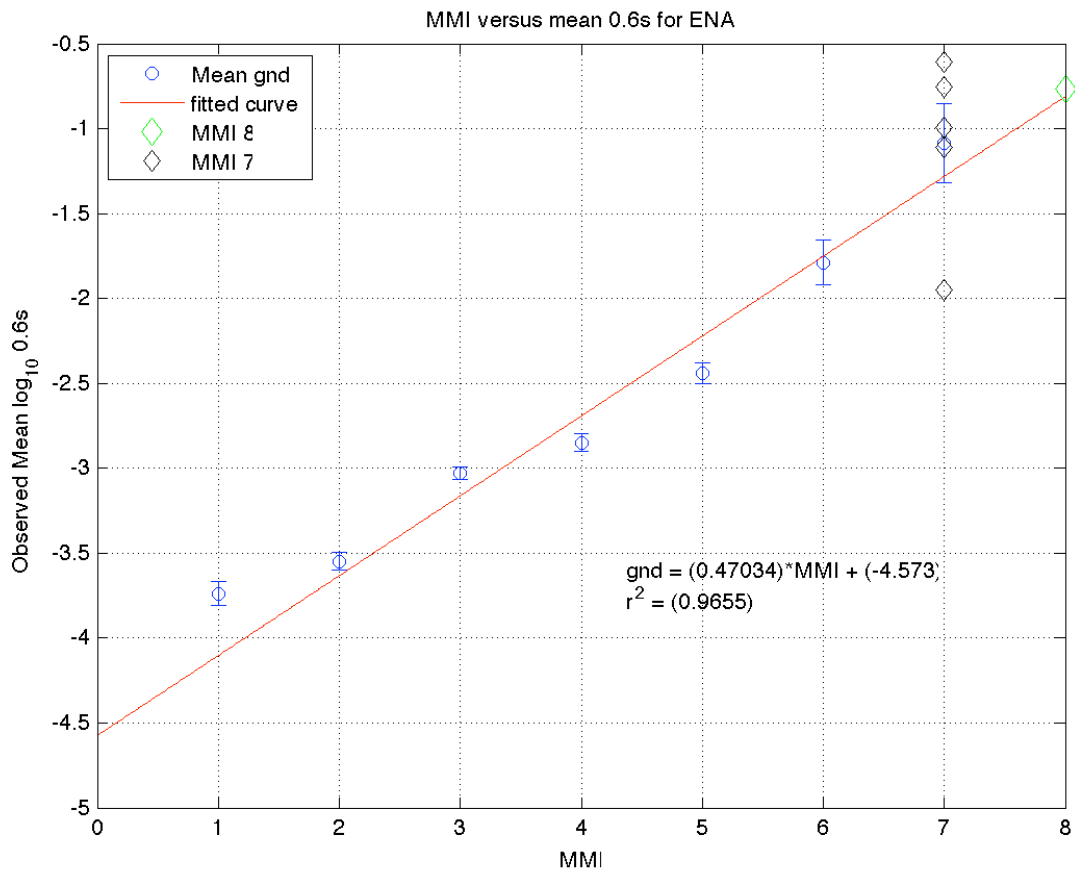


Figure A8: 0.6 s Sa regression for Equation A1 plotted with median logGM and its 95% confidence limits plus logGM values for MMI VII and VIII.

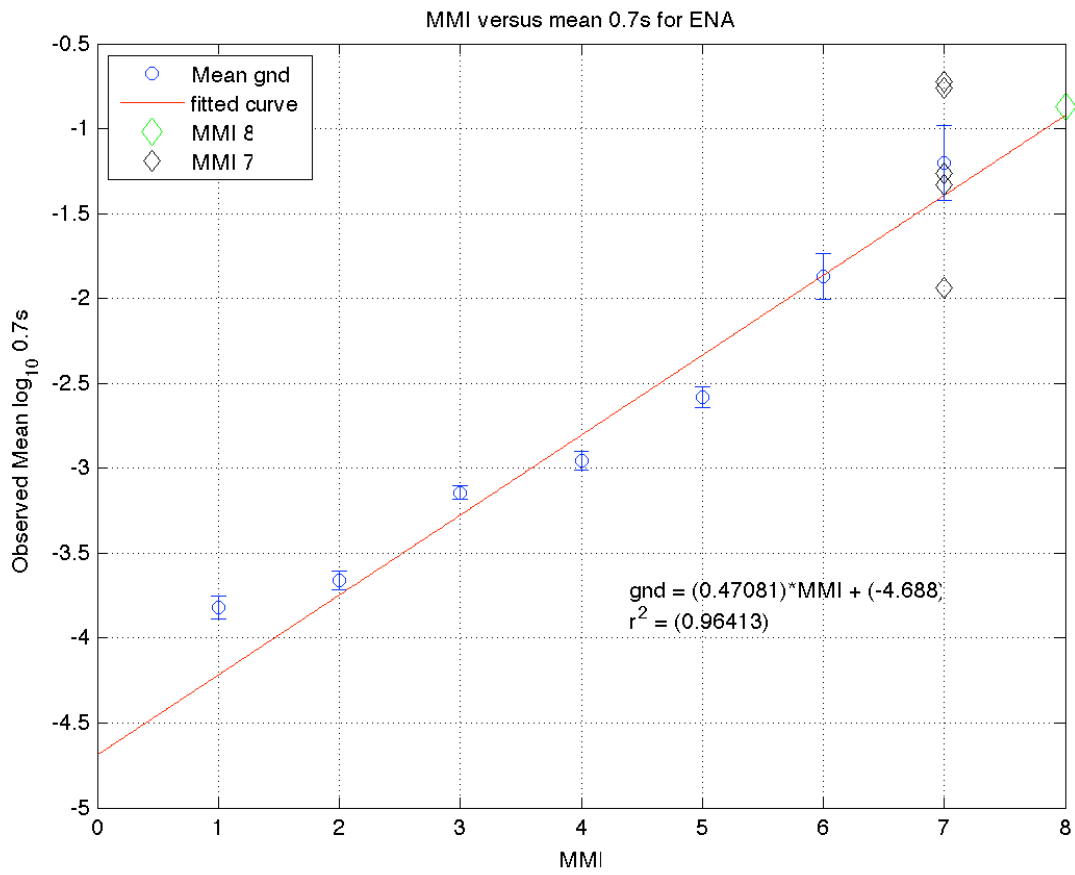


Figure A9: 0.7 s Sa regression for Equation A1 plotted with median logGM and its 95% confidence limits plus logGM values for MMI VII and VIII.

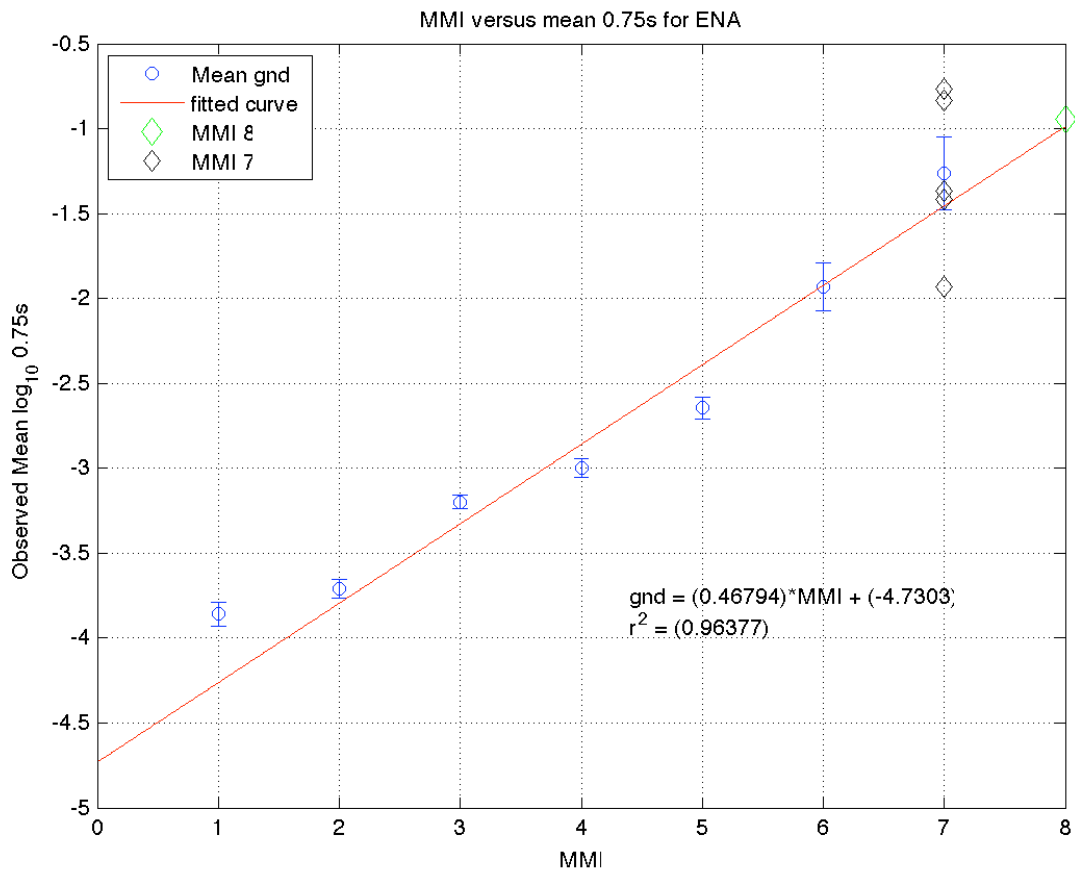


Figure A10: 0.75 s Sa regression for Equation A1 plotted with median logGM and its 95% confidence limits plus logGM values for MMI VII and VIII.

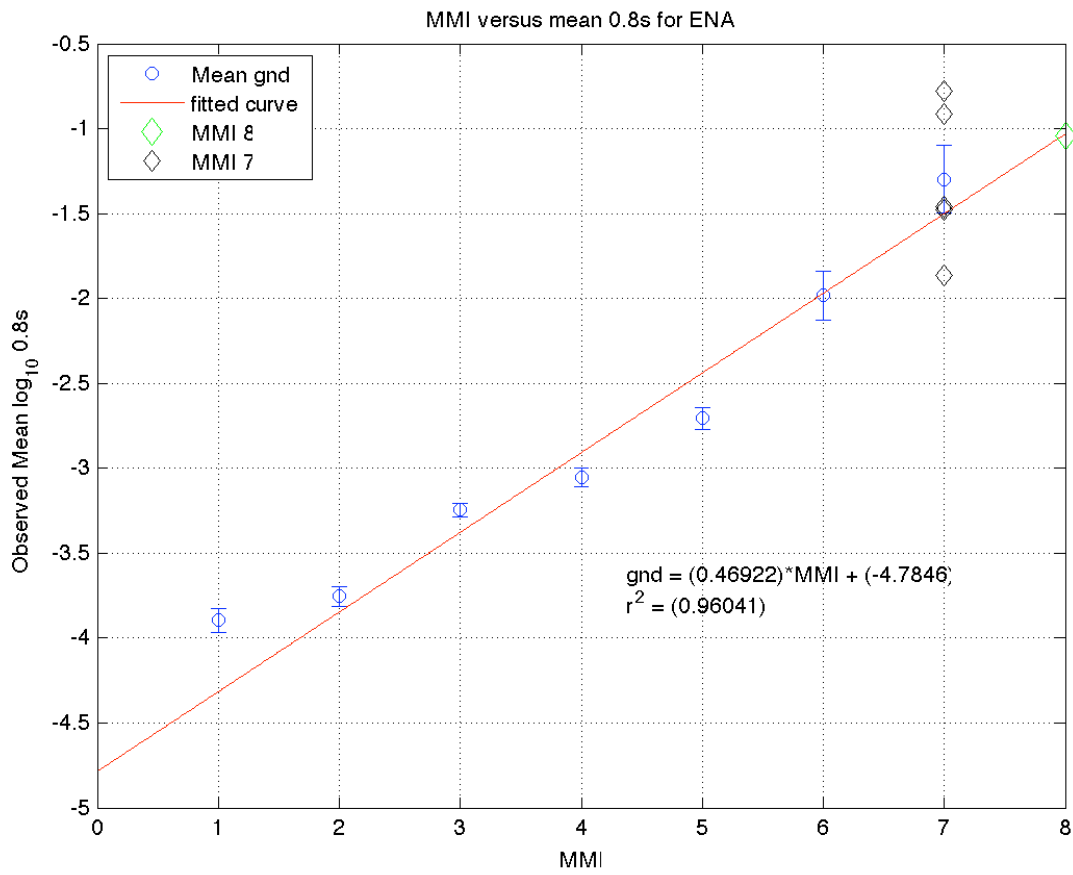


Figure A11: 0.8 s Sa regression for Equation A1 plotted with median logGM and its 95% confidence limits plus logGM values for MMI VII and VIII.

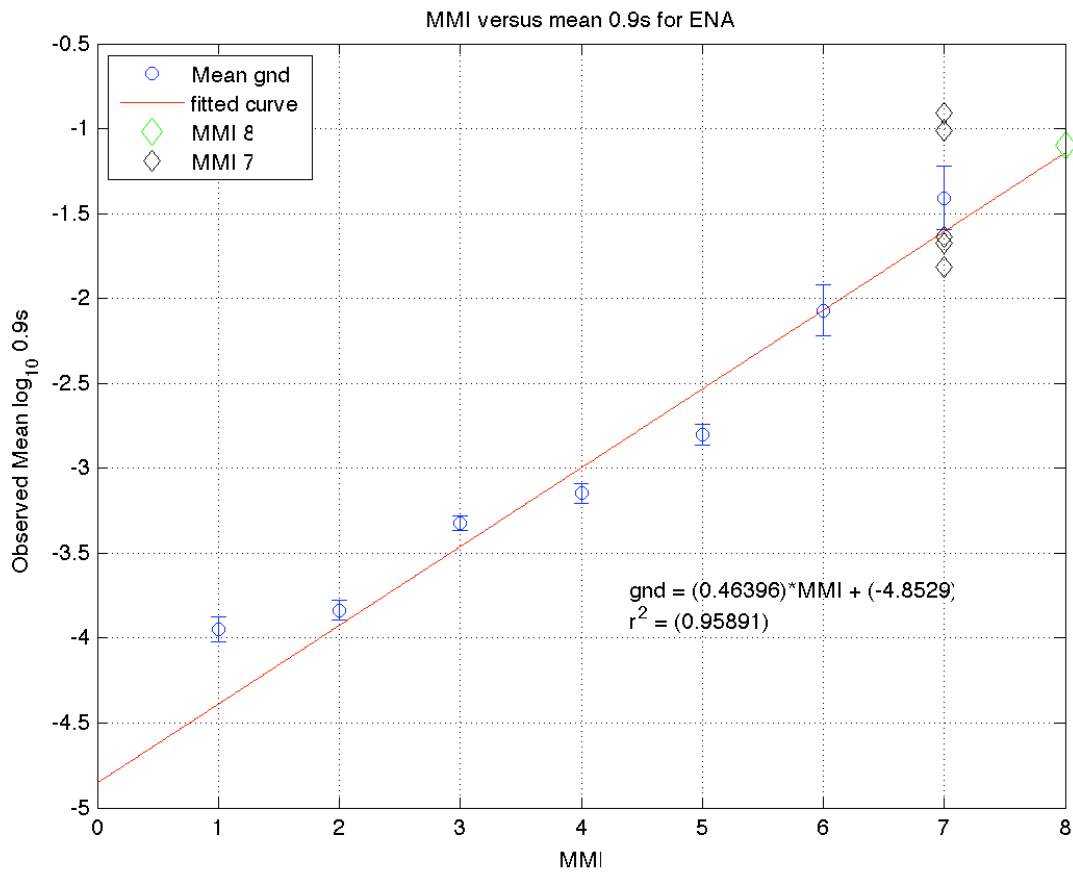


Figure A12: 0.9 s Sa regression for Equation A1 plotted with median logGM and its 95% confidence limits plus logGM values for MMI VII and VIII.

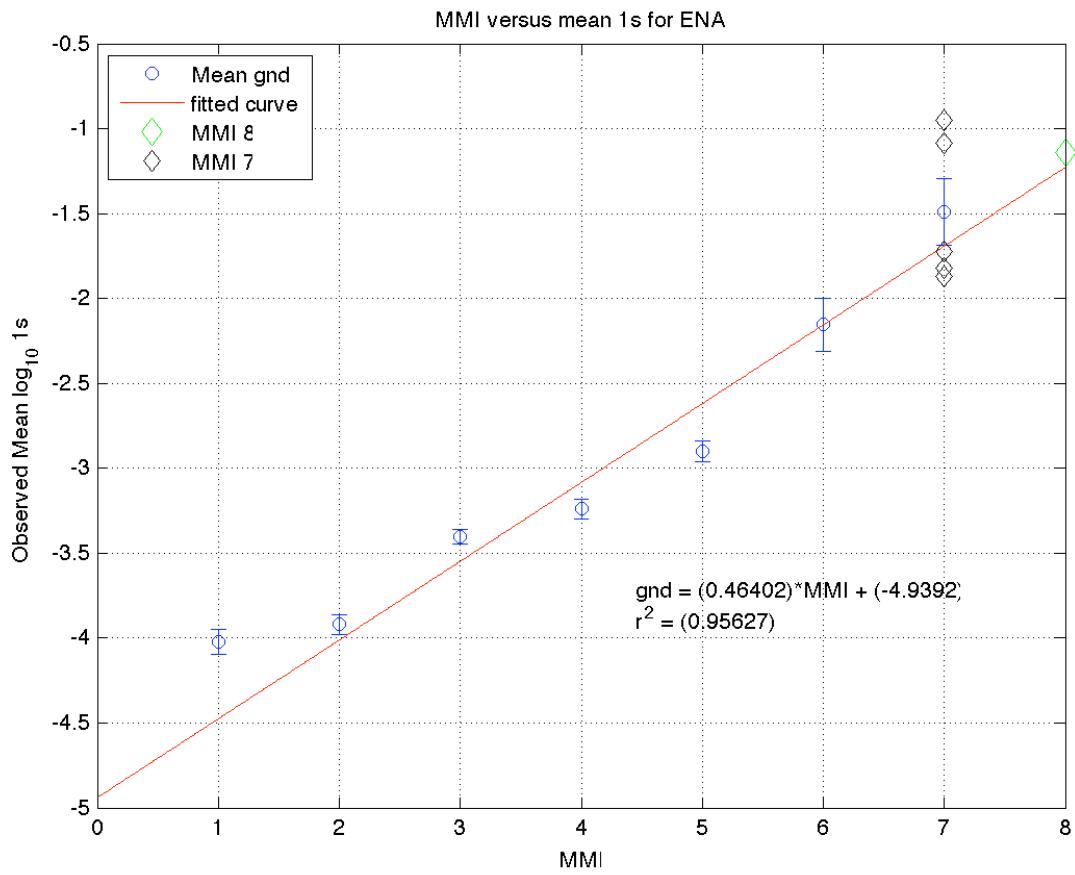


Figure A13: 1.0 s Sa regression for Equation A1 plotted with median logGM and its 95% confidence limits plus logGM values for MMI VII and VIII.

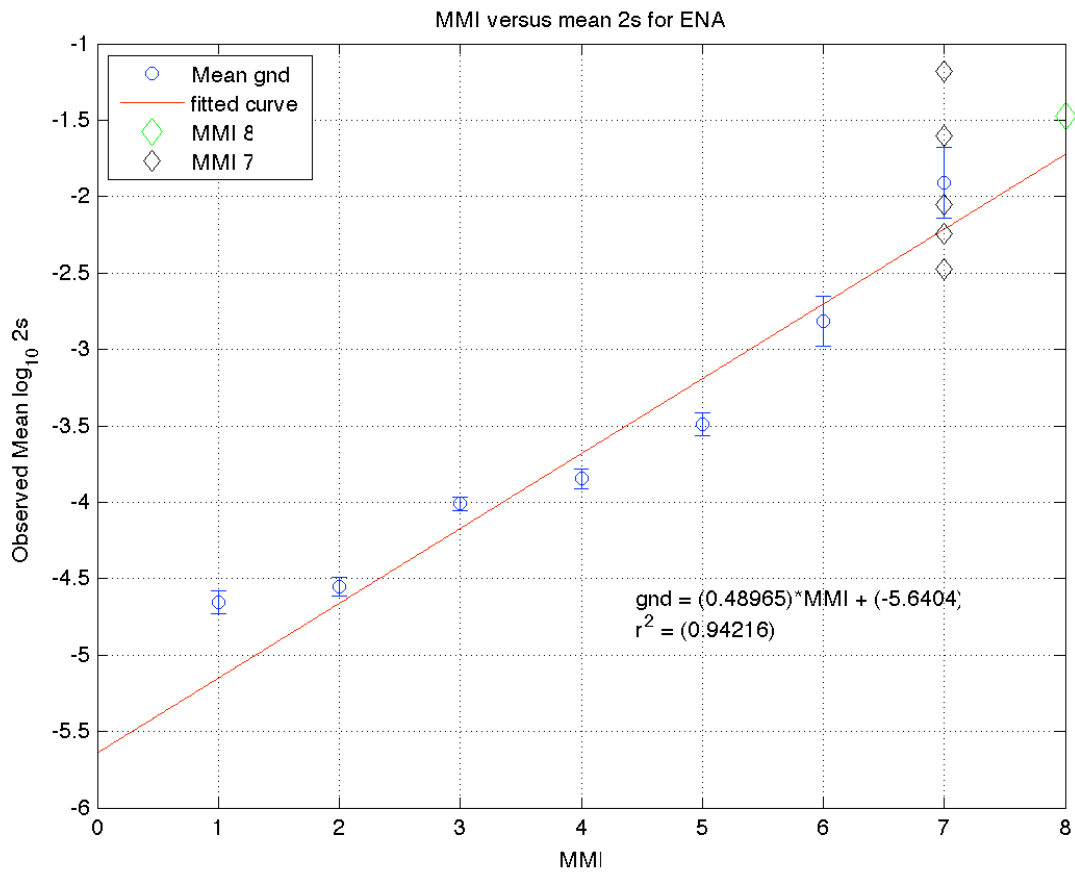


Figure A14: 2.0 s Sa regression for Equation A1 plotted with median logGM and its 95% confidence limits plus logGM values for MMI VII and VIII.

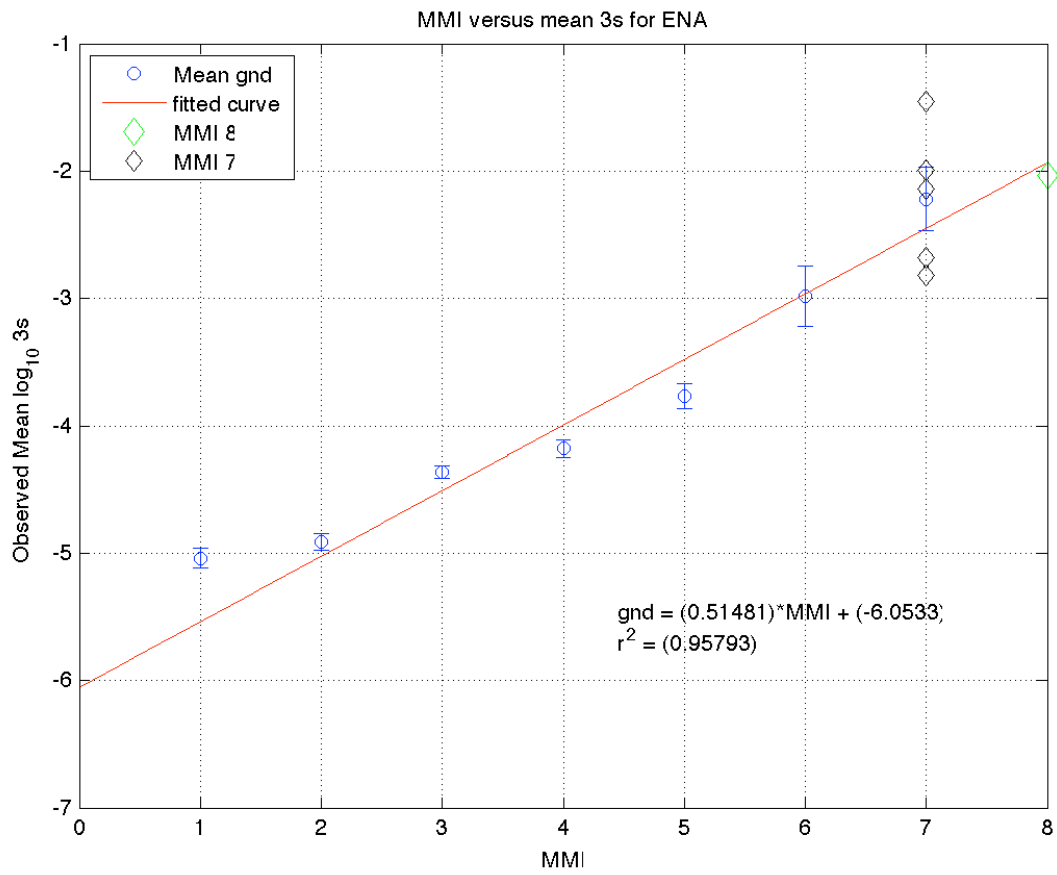


Figure A15: 3.0 s Sa regression for Equation A1 plotted with median logGM and its 95% confidence limits plus logGM values for MMI VII and VIII.

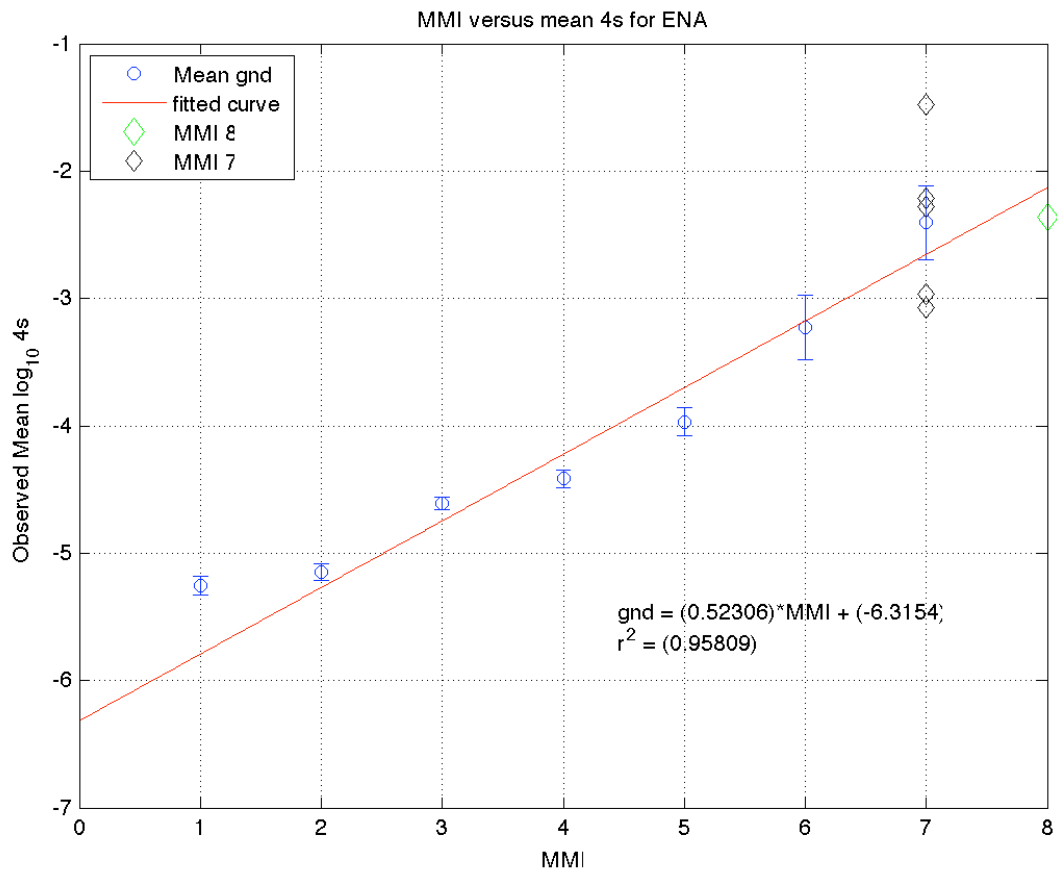


Figure A16: 4.0 s Sa regression for Equation A1 plotted with median logGM and its 95% confidence limits plus logGM values for MMI VII and VIII.

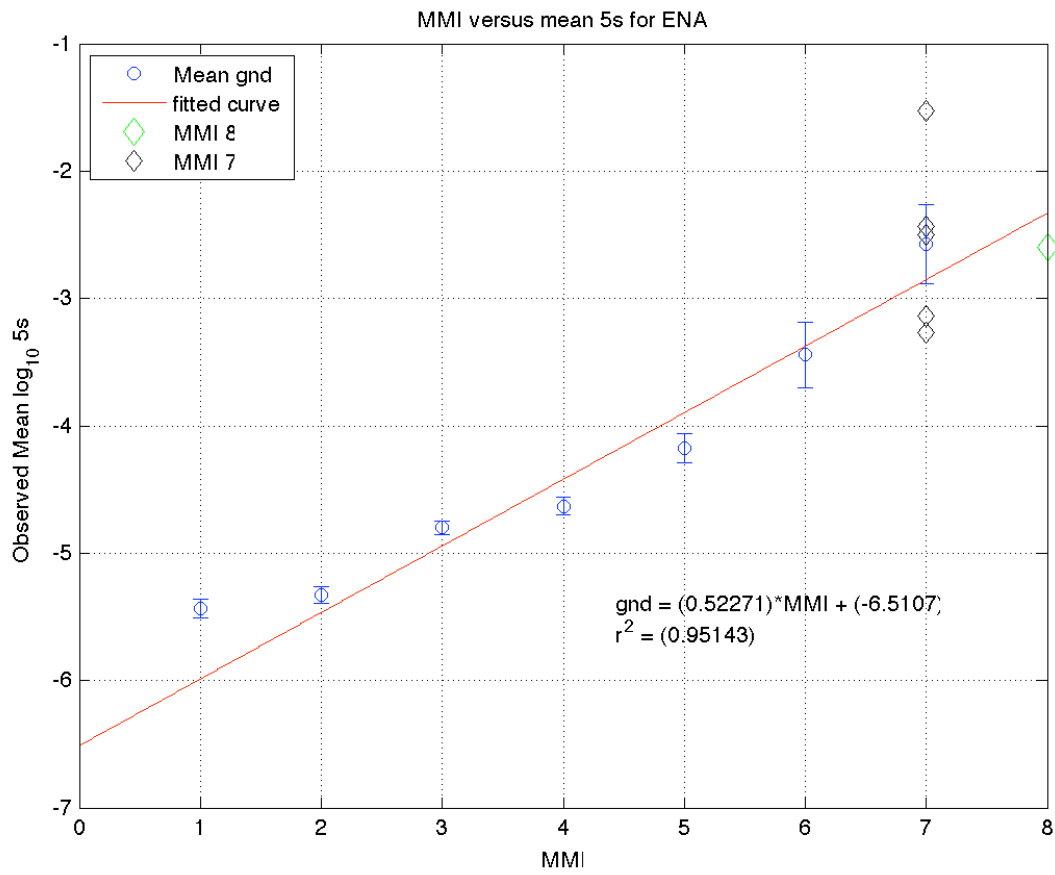


Figure A17: 5.0 s Sa regression for Equation A1 plotted with median logGM and its 95% confidence limits plus logGM values for MMI VII and VIII.

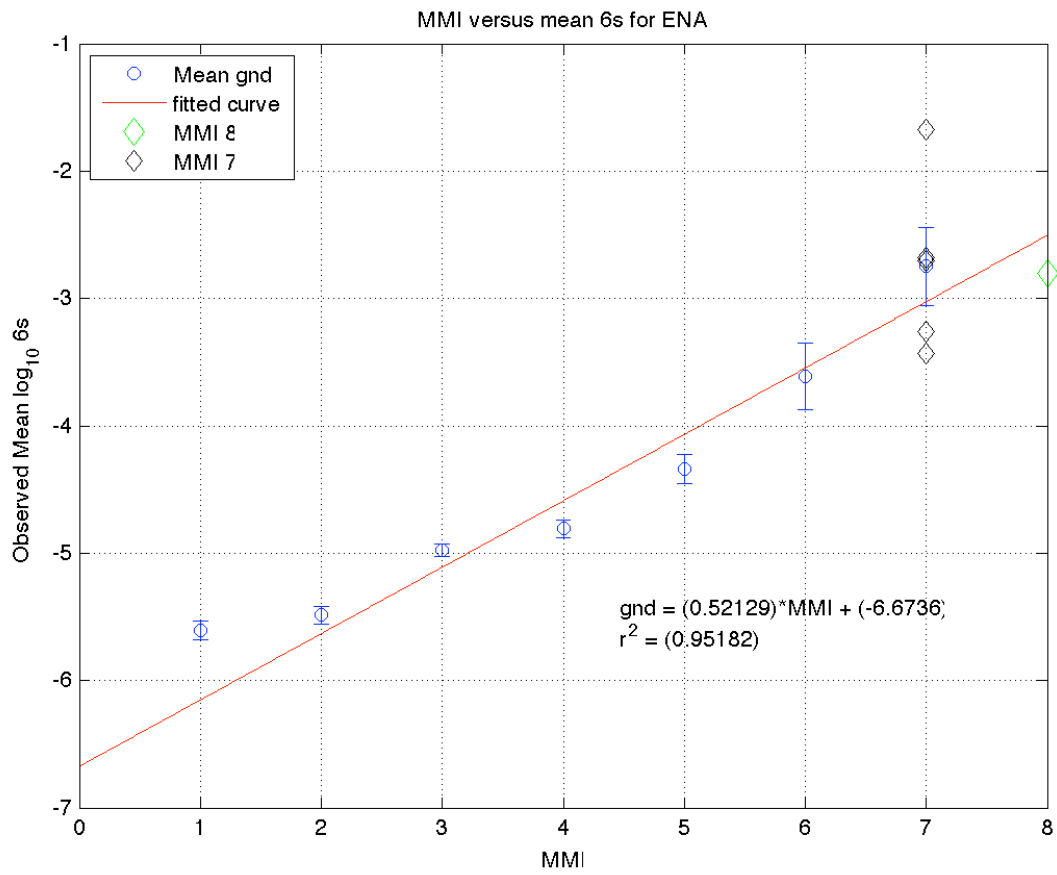


Figure A18: 6.0 s Sa regression for Equation A1 plotted with median logGM and its 95% confidence limits plus logGM values for MMI VII and VIII.

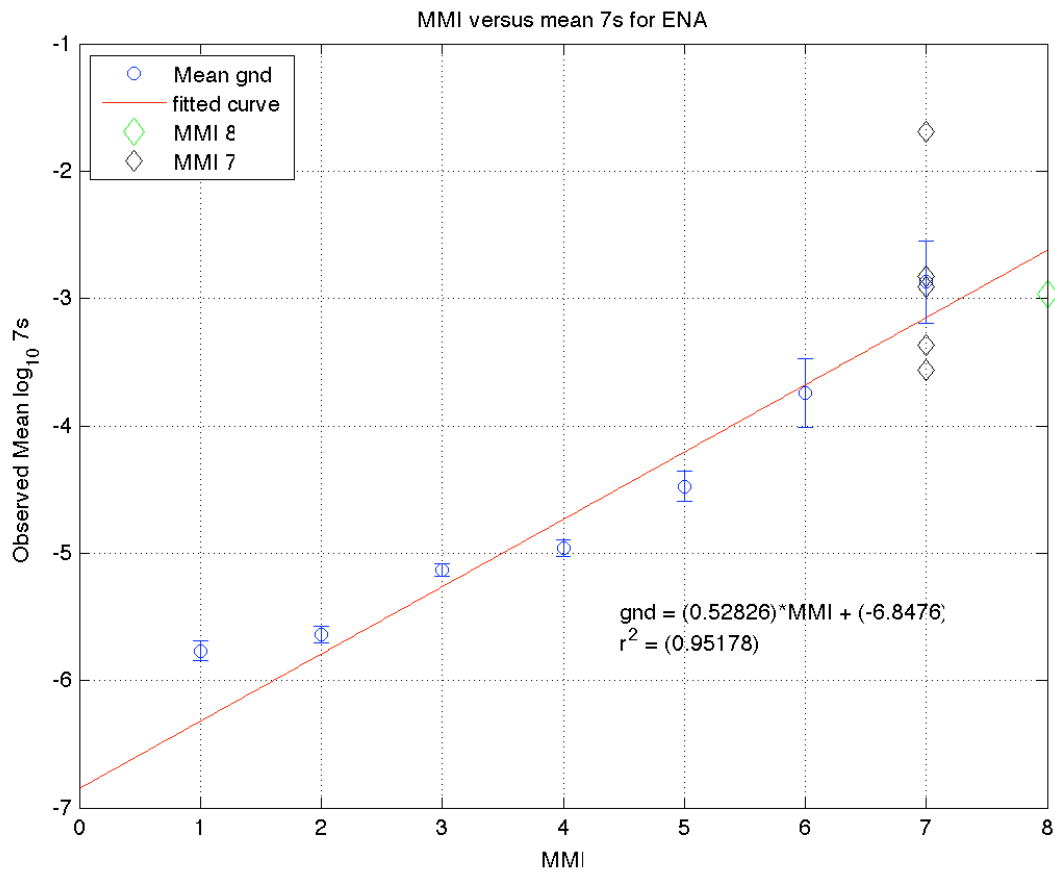


Figure A19: 7.0 s Sa regression for Equation A1 plotted with median logGM and its 95% confidence limits plus logGM values for MMI VII and VIII.

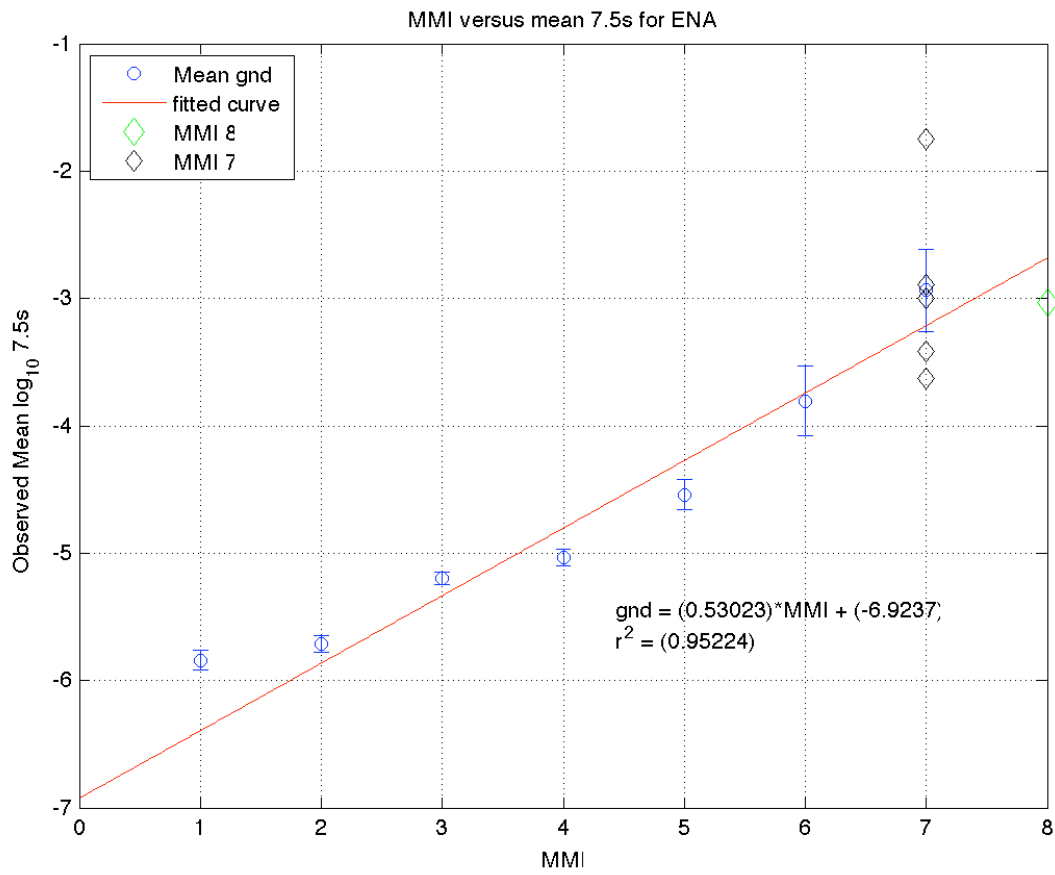


Figure A20: 7.5 s Sa regression for Equation A1 plotted with median logGM and its 95% confidence limits plus logGM values for MMI VII and VIII.

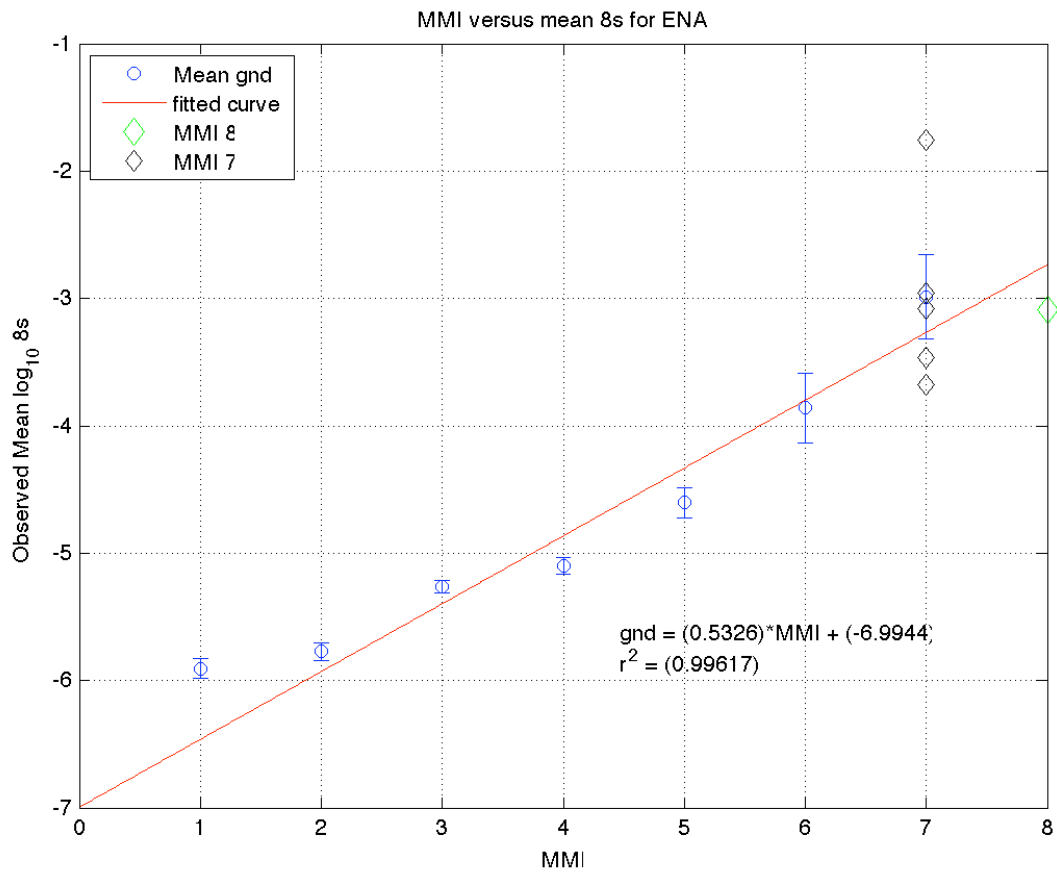


Figure A21: 8.0 s Sa regression for Equation A1 plotted with median logGM and its 95% confidence limits plus logGM values for MMI VII and VIII.

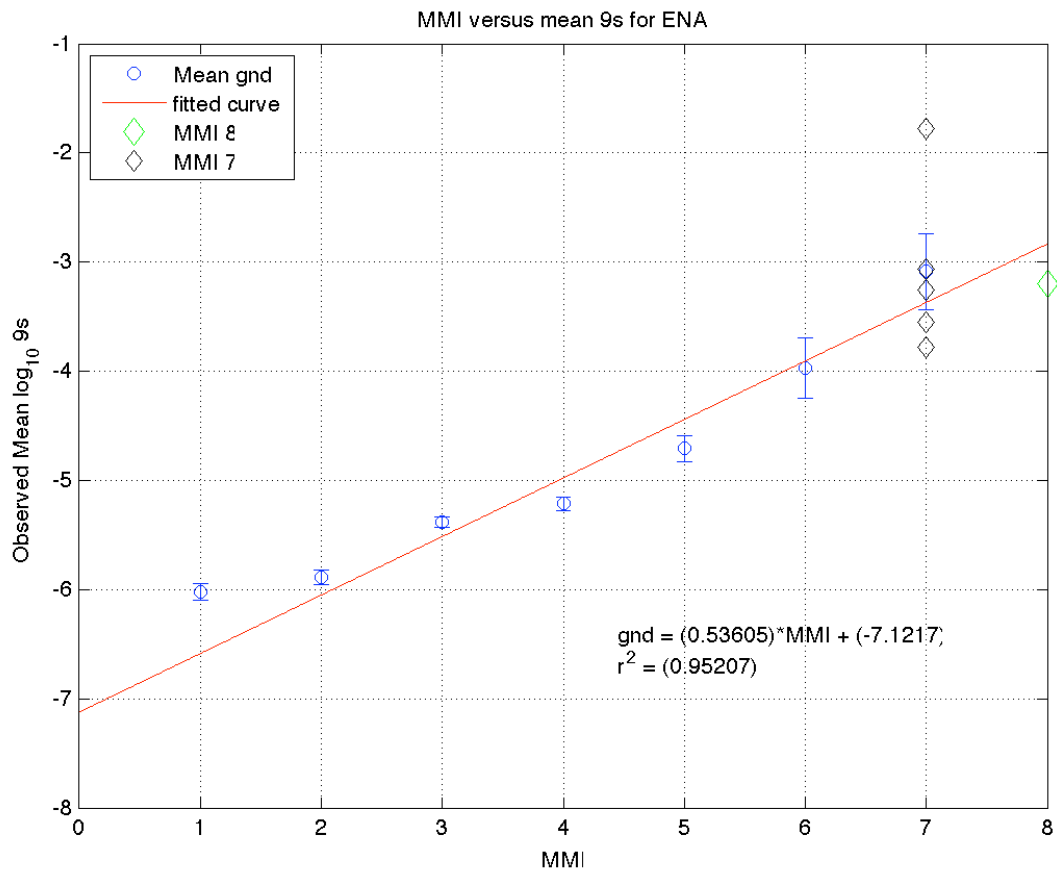


Figure A22: 9.0 s Sa regression for Equation A1 plotted with median logGM and its 95% confidence limits plus logGM values for MMI VII and VIII.

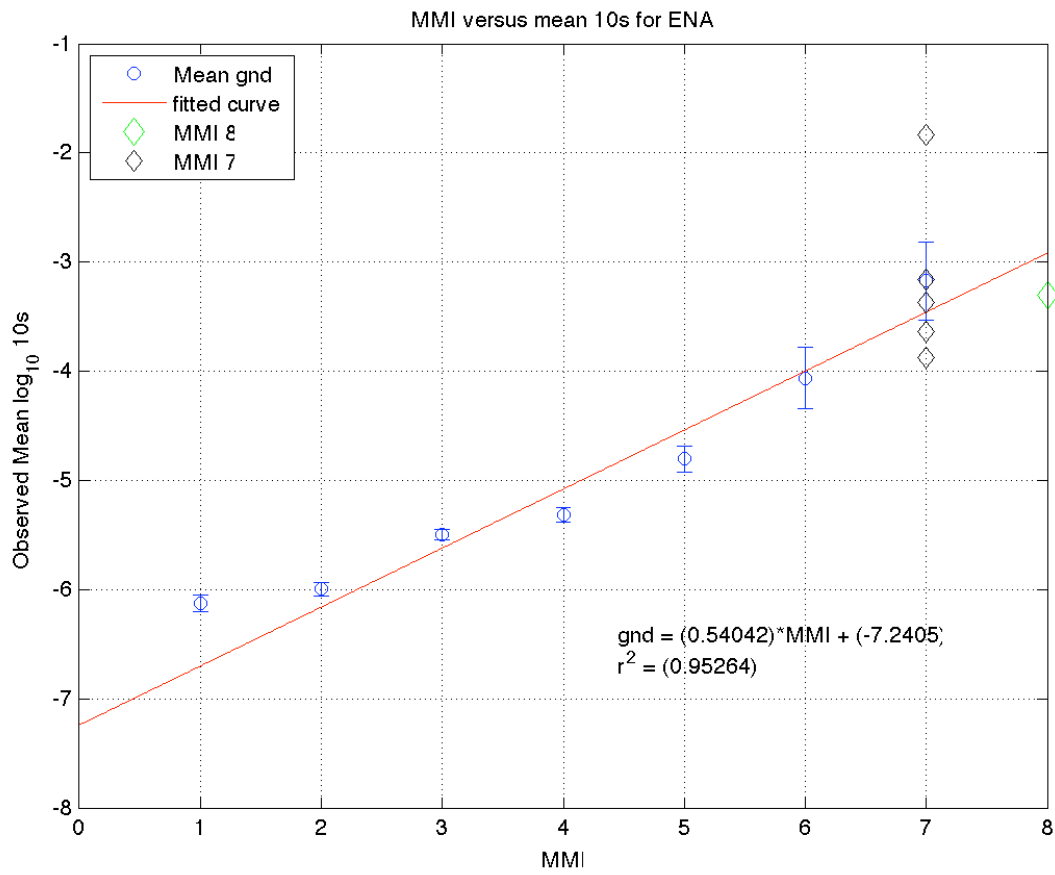


Figure A23: 10. s Sa regression for Equation A1 plotted with median logGM and its 95% confidence limits plus logGM values for MMI VII and VIII.